Redox-linked protonation state changes in cytochrome bc_1 identified by Poisson–Boltzmann electrostatics calculations

Astrid R. Klingen [a], Hildur Palsdottir [b,1], Carola Hunte [b], G. Matthias Ullmann [a,*]

[a] Structural Biology/Bioinformatics Group, University of Bayreuth, Germany
[b] Department of Molecular Membrane Biology, Max Planck Institute of Biophysics, Frankfurt am Main, Germany

Abstract

Cytochrome bc_1 is a major component of biological energy conversion that exploits an energetically favourable redox reaction to generate a transmembrane proton gradient. Since the mechanistic details of the coupling of redox and protonation reactions in the active sites are largely unresolved, we have identified residues that undergo redox-linked protonation state changes. Structure-based Poisson–Boltzmann/Monte Carlo titration calculations have been performed for completely reduced and completely oxidised cytochrome bc_1. Different crystallographically observed conformations of Glu272 and surrounding residues of the cytochrome b subunit in cytochrome bc_1 from *Saccharomyces cerevisiae* have been considered in the calculations. Coenzyme Q (CoQ) has been modelled into the CoQ oxidation site (Q_o-site). Our results indicate that both conformational and protonation state changes of Glu272 of cytochrome b may contribute to the postulated gating of CoQ oxidation. The Rieske iron–sulphur cluster could be shown to undergo redox-linked protonation state changes of its histidine ligands in the structural context of the CoQ-bound Q_o-site. The proton acceptor role of the CoQ ligands in the CoQ reduction site (Q_i-site) is supported by our results. A modified path for proton uptake towards the Q_i-site features a cluster of conserved lysine residues in the cytochrome b (Lys228) and cytochrome c_1 subunits (Lys288, Lys289, Lys296). The cardiolipin molecule bound close to the Q_i-site stabilises protons in this cluster of lysine residues.
© 2007 Elsevier B.V. All rights reserved.

1. Introduction

The cytochrome bc_1 complex (cytochrome bc_1) is a key enzyme of biological energy conversion in bacteria and mitochondria. It is a multi-subunit transmembrane protein complex that transfers electrons from reduced coenzyme Q (CoQ) to a mobile redox-active protein and translocates protons

across the membrane. The free energy of the catalysed redox reaction is converted into the energy of a transmembrane proton motive force. In mitochondria, cytochrome bc_1 spans the inner mitochondrial membrane and transfers electrons from ubiquinol to cytochrome c. Mitochondrial cytochrome bc_1 represents complex III of the respiratory chain.

The coupling between electron transfer and proton translocation in cytochrome bc_1 is based on the so-called modified Q-cycle mechanism (Fig. 1) [1–3]. The mechanism requires two CoQ-binding sites and a site for cytochrome c reduction, connected by chains of protein-bound redox cofactors. Three different subunits of the complex form the catalytic sites and bind the cofactors: cytochrome b, cytochrome c_1, and the Rieske iron–sulphur protein (ISP). The oxidation of CoQ is catalysed in the so-called Q_o-site of the complex: the reduced and protonated quinol form of CoQ is converted into the oxidised and deprotonated quinone form. The two electrons of this reaction are transferred to two different electron acceptor groups, namely
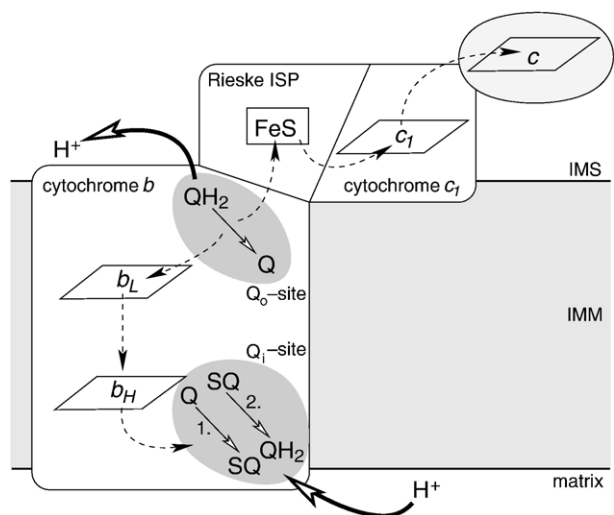
Fig. 1. The Q-cycle mechanism of cytochrome bc_1. Protons from the oxidation of quinol in the Q_o-site are set free to the intermembrane space. One electron from the oxidation of quinol is transferred via the high-potential chain of redox cofactors ([Fe_2S_2] cluster of the Rieske ISP subunit and haem c_1 of cytochrome c_1) to cytochrome c. The second electron is recycled back into the CoQ pool: it is transferred to the Q_i-site via the low-potential chain of redox cofactors (haem b_L and b_H of cytochrome b). Two molecules of CoQ have to get oxidised in the Q_o-site to provide the two electrons for complete reduction of one CoQ molecule in the Q_i-site. $QH_2 + 2$ cyt $c(ox) + 2$ $H_{matrix}^+ \rightarrow Q + 2$ cyt $c(red) + 4$ H_{IMS}^+ is the overall reaction catalysed by cytochrome bc_1. Electron transfer is indicated by dashed arrows, proton translocation by bold arrows. Q—oxidised CoQ, quinone. QH_2—reduced CoQ, quinol. SQ—stable semiquinone intermediate in the Q_i-site. ISP—iron–sulphur protein. IMS—mitochondrial inter-membrane space, IMM—inner mitochondrial membrane.

a *b*-type haem group (haem b_L, bound to the cytochrome b subunit of the complex) and a Rieske [Fe_2S_2] iron–sulphur cluster (bound to the ISP subunit). By movement of its mobile head domain [4], the Rieske ISP then transfers an electron to the haem c_1 group bound to the cytochrome c_1 subunit of cytochrome bc_1. Cytochrome c_1 finally reduces the *c*-type haem group of the substrate cytochrome c. The second electron of the oxidation of CoQ is transferred via haem b_L and haem b_H of cytochrome b to the so-called Q_i-site. In the Q_i-site, oxidised CoQ gets reduced to semiquinone and finally to quinol by two electrons sequentially arriving from the Q_o-site. Since CoQ oxidation and reduction are coupled to proton release and uptake, respectively, the location of the two CoQ-binding sites relative to the membrane links electron transfer to the translocation of protons across the membrane.

Although the overall scheme of the Q-cycle mechanism is widely accepted, details of the reactions in the catalytic sites remain largely unresolved [5,6]. Among the most heavily debated aspects of cytochrome bc_1 catalysis are the nature of proton acceptor and donor groups [7–11], the nature of the rate-limiting steps [12,13], the sequence of single proton and electron transfer steps [12,14], the mechanistic basis of the bifurcation of electron transfer pathways in the Q_o-site [13–18], and the control of harmful bypass reactions [19–21]. Considerable effort has been made to clarify these mechanistic details. However, this effort resulted in the formulation of different

mechanistic models that are based on often conflicting interpretation of the available experimental data.

To evaluate the conflicting models of Q_o- and Q_i-site catalysis, it is necessary to identify redox-linked protonation state changes in cytochrome bc_1, because redox-linked protonation state changes are at the very heart of any mechanism coupling electron and proton transfer reactions. Several recent Fourier transform infrared (FTIR) spectroscopy studies [22–27] have successfully embarked on identifying redox-linked protonation state changes in cytochrome bc_1. In this work, we report redox-linked protonation state changes of cytochrome bc_1 that have been identified from Poisson–Boltzmann/Monte Carlo titration calculations. The calculations are based on the crystal structures of cytochrome bc_1 from the yeast *Saccharomyces cerevisiae* [28–30]. The conformational variability of the Q_o-site observed in different crystal structures has been taken into account. For different redox states of the complex that correspond to the experimental conditions of the FTIR studies we obtain protonation probabilities for all titratable groups in the protein complex.

In the following, we give some basic theoretical background and describe the setup of our calculations. We then present and discuss the redox-linked protonation state changes revealed by our calculations. A small number of titratable residues were identified that have markedly different protonation probabilities in the fully oxidised and fully reduced state of the complex. Our results support the idea that conformational variability of the Q_o-site plays a role during CoQ oxidation. We observe a coupling between protonation reactions and conformational transitions that may be the basis of the recently discussed gating of the Q_o-site reaction [6,19,20]. Concerning the Q_i-site, our results propose a modified path for proton uptake to the active site.

2. Material and computational setup

2.1. Preparation of the crystal structures

Our calculations are based on two different crystal structures of cytochrome bc_1 from *S. cerevisiae*. These structures contain the Q_o-site inhibitors stigmatellin (PDB code 1KB9, 2.3 Å resolution, Ref. [29]) and hydroxydioxobenzothiazole (HDBT, PDB code 1P84, 2.5 Å resolution, Ref. [30]), respectively. The HDBT-inhibited structure contains an additionally refined second cardiolipin molecule [31]. Both crystal structures comprise nine different subunits. Two copies of each subunit form the dimeric state of the complex, which is considered to be the catalytically active state of cytochrome bc_1 [32].

In both crystal structures, the Rieske head domain is found in its so-called *b*-position, forming the Q_o-site together with the cytochrome b subunit.

The crystal structures were prepared for the Poisson–Boltzmann (PB) calculations using the molecular modelling package CHARMM [33]. All lipids, detergent and water molecules were retained during the structure preparations. The desired redox states of the complex were introduced by assigning appropriate partial charges to the atoms of the redox cofactors. Hydrogen atom positions were constructed and subsequently energy-minimised using the steepest decent (SD) and conjugate gradient (CG) techniques and short molecular dynamics simulations as implemented in CHARMM. The minimisation consisted of 1000 SD steps, 500 MD steps of 0.2 fs at 100 K, 500 MD steps of 0.5 fs at 200 K, 500 MD steps of 1 fs at 300 K, 500 MD steps of 1 fs at 100 K, 1000 SD steps and 2000 CG steps. The procedure was followed for all states of the system that were treated in separate PB-calculations. The crystal structures contain antibody fragments, which bind to the Rieske protein head domain and were used for cocrystallisation. These antibody fragments were not included in our

calculations: test calculations showed, that their removal from the structure has negligible effect on the protonation probabilities of cytochrome bc_1.

2.2. Modelling of undecylstigmatellin and CoQ into the Q_o-site

In order to obtain results that can be compared to the FTIR data published by Ritter et al. [25], we have performed calculations on cytochrome bc_1 inhibited by undecylstigmatellin (UST). For these calculations, we have used the stigmatellin-inhibited structure of cytochrome bc_1 from *S. cerevisiae*. Since the crystal structure contains stigmatellin A which has a different hydrophobic tail than UST (Fig. 2A and B), we have changed the hydrophobic tail of stigmatellin A into the simple alkyl chain of UST. The hydrophobic tail of UST in the Q_o-site has been energy minimised using CHARMM. The details of the minimisation procedure are the same as for the minimisation of the hydrogen atom positions described above. Since Ritter et al. [25] have reported changes in the redox state of UST in the Q_o-site of cytochrome bc_1, we consider two different redox states of UST in our calculations. The probable chemical structures of oxidised and reduced UST are shown in Fig. 2B and C, respectively. For both redox states, we have calculated partial charges using a density functional theory (DFT) approach (see Supplementary Material).

To obtain mechanistically relevant results, we have performed calculations on cytochrome bc_1 with the substrate CoQ modelled into the Q_o-site. Since the available crystal structures of cytochrome bc_1 do not contain CoQ in the Q_o-site, we have followed a modelling procedure that uses structural information available for another CoQ-binding site, namely the Q_B-site of the photosynthetic reaction centre. The reaction centre has been crystallised with stigmatellin (PDB code 4PRC) and with CoQ (PDB code 2PRC) in the active site [34]. The binding mode of stigmatellin is very similar in the Q_o-site and the Q_B-site. In both sites, the carbonyl oxygen atom of the chromone ring system of oxidised stigmatellin forms a hydrogen bond towards the nitrogen atom of a histidine sidechain. The same histidine sidechain coordinates an iron atom with its other nitrogen atom (the mononuclear iron centre in the reaction centre and the Rieske cluster in cytochrome bc_1). The hydroxy group of the chromone ring system interacts with an oxygen-containing sidechain (serine in the reaction centre, glutamate in cytochrome bc_1. Using the relative orientation of stigmatellin and CoQ observed in the crystal structures of the reaction centre, and the position of stigmatellin in the Q_o-site of cytochrome bc_1, we derive the position of CoQ in the Q_o-site of cytochrome bc_1 from yeast. Starting from this similarity-based initial positioning, we have performed an energy minimisation of the hydrophobic tail of CoQ using CHARMM, during which only minor structural changes are observed. The details of the minimisation procedure are the same as for the minimisation of hydrogen atom positions described above. The tail was modelled to contain one isopren unit. In the framework of the single-occupancy model [35] we have by this procedure obtained a reasonable working model of CoQ in the Q_o-site (Fig. 3). In all calculations, the Q_i-site contains CoQ as observed in both crystal structures from *S. cerevisiae*.

2.3. Addition of a model membrane

To account for the effect of the membrane environment on the electrostatics of cytochrome bc_1 we have added a model membrane around the crystal structures prepared for the PB-calculations. The membrane is modelled by a torus-shaped belt of uncharged atoms, placed with HLINK from the TRIP program package [36]. For the PDB deposited coordinates, the membrane model extends from $y_{\text{interface matrix}} = -61$ Å to $y_{\text{interface intermembrane space}} = -39$ Å along the membrane normal of the complex. In the PB-calculations, a low dielectric constant is assigned to the volume occupied by the uncharged membrane atoms, which thus adequately represent the hydrophobic core of the membrane. Explicit water molecules were removed from the structures for PB-calculation after addition of the model membrane.

2.4. Treatment of conformational variability in the Q_o-site

As obvious from the crystal structures from *S. cerevisiae*, the Q_o-site of cytochrome bc_1 adopts different conformations in presence of the Q_o-site
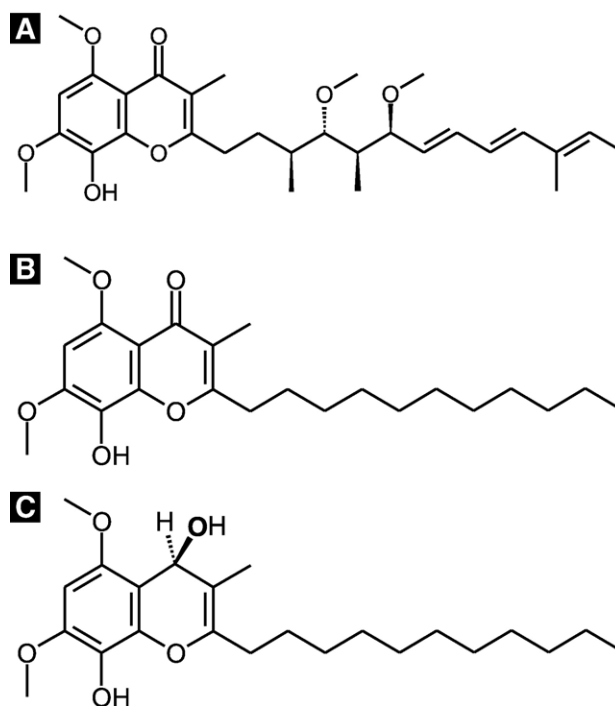

Fig. 2. (A) Chemical structure of stigmatellin A contained in the crystal structure of cytochrome bc_1 from *S. cerevisae*. (B) Chemical structure of oxidised undecylstigmatellin (UST). (C) Chemical structure of reduced UST. The position of the highlighted oxygen atom (bold font) has been energy minimised during the structure preparation procedure, in order obtain an appropriate tetrahedral geometry at the corresponding ring carbon atom.

inhibitors stigmatellin and HDBT. In both crystal structures, the Rieske head domain is found in its so-called *b*-position forming the Q_o-site together with the cytochrome *b* subunit [4]. The most obvious difference between the structures is the orientation of the sidechain of E272^{CYB} (Fig. 3). E272^{CYB} points towards the Rieske cluster in the stigmatellin-inhibited complex (referred to as conformation Glu-FeS), and points towards haem b_L in the HDBT-inhibited complex (referred to as conformation Glu-*b*). Differences between the two conformations are limited to residues 265 to 273 of cytochrome *b* and the sidechain of H253^{CYB}. We assume that the rest of the complex adopts the conformation observed in the HDBT-inhibited crystal structure and we keep it fixed in this conformation during the Monte Carlo calculations. The energy difference between the two conformations (shown in green and purple in Fig. 3) in presence of CoQ in the active site has been estimated by a combined molecular mechanics/Poisson–Boltzmann approach that is detailed in the Supplementary Material. The value for the conformational energy difference enters into the Monte Carlo calculations that reveal to which extent the two conformations are populated in the complex with CoQ in the Q_o-site (see below).

2.5. Calculation of protonation probabilities

To characterise protonation probabilities as well as the probabilities of the different Q_o-site conformations, we have performed PB electrostatics and Metropolis Monte Carlo (MC) titration calculations. The underlying theory is described in detail in Ref. [37] and [38].

The PB-calculations were performed using multiflex from the MEAD package [39]. The results describe the energetics of all N titratable groups in cytochrome bc_1 in terms of N intrinsic pK-values and a symmetric $N \times N$ matrix of pairwise interaction energies. The intrinsic pK-values are calculated as shifts relative to experimentally determined pK-values of appropriate model reactions in aqueous solution (see Supplementary Material). In our calculations, all aspartate, glutamate, lysine, arginine, histidine, tyrosine and cysteine residues, the propionate moieties of the haem groups and the lipid head-groups were considered titratable. Apart from the Rieske ligand histidines, sidechains that are involved in covalent or coordination bonds are not considered titratable.
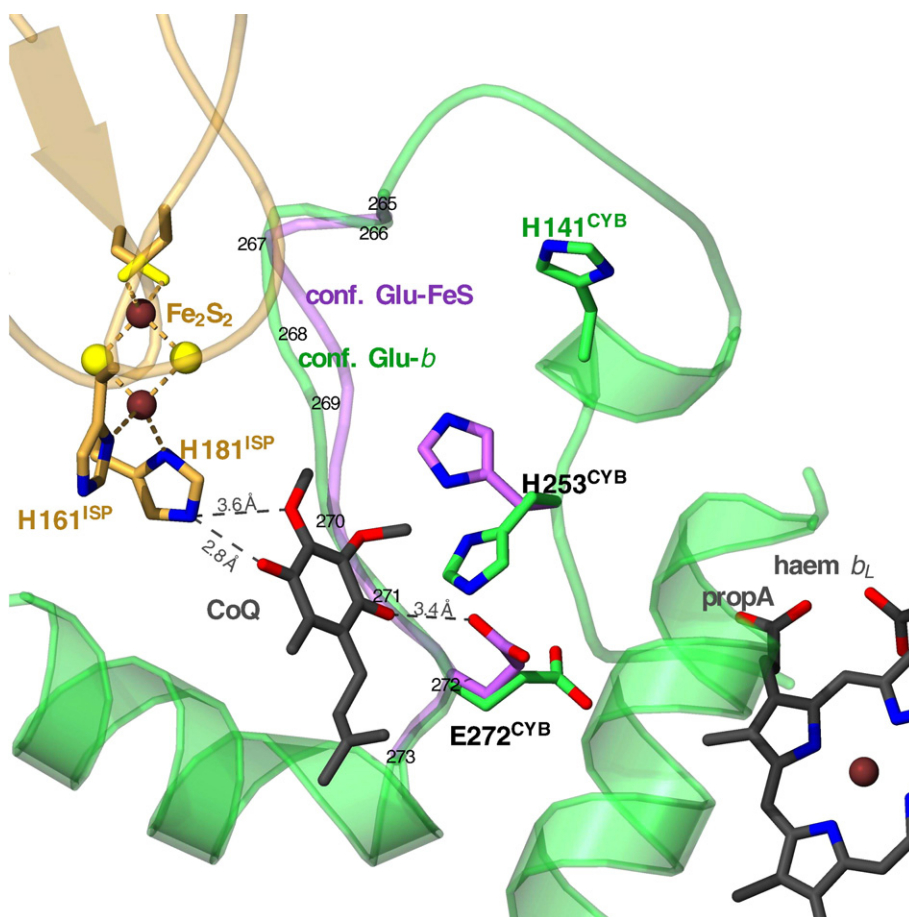
Fig. 3. The substrate CoQ modelled into the Q_o-site of cytochrome bc_1. The Q_o-site is formed by two of the three catalytic subunits of the cytochrome bc_1 complex, namely cytochrome b (CYB, coloured in green) and the Rieske iron–sulphur protein (ISP, coloured in ochre). Different conformations of the Q_o-site as observed in the presence of stigmatellin (coloured in purple: conformation Glu-FeS, Ref. [28]) and HDBT (coloured in green: conformation Glu-b, Ref. [31]) have been considered in the calculation of protonation probabilities in presence of CoQ in the Q_o-site. Differences between the two conformations are limited to residues 265 to 273 of cytochrome b (the positions of the C_α-atoms in this fragment are labelled by their residue numbers), and the sidechain of H253^{CYB}. Coordinates outside these regions are virtually identical in the two structures, and coordinates from the HDBT-inhibited structure have been used for the rest of the complex. The two electron acceptors of the CoQ oxidation reaction (haem b_L and the Rieske cluster), the cysteine and histidine ligands of the Rieske cluster, and residues undergoing redox-linked changes in their titration behaviour are highlighted. Distances between atoms are given to detail the orientation of CoQ modelled into the active site.

Histidines are treated as described by Bashford et al. [40]. N- and C-termini are considered titratable as far as they are resolved in the crystal structures. Unresolved termini are the N-terminus of the small subunits 6, 7, 8 and 9, and the C-terminus of cytochrome c_1 and the small subunit 9. The effect of these unresolved termini is considered marginal. Because of their structural flexibility they can be expected to be well solvated. Their charges are consequently well shielded and have little effect on the titration behaviour in the rest of the complex. Neutral blocking groups were attached to replace the unresolved termini.

In contrast to all other titratable groups, model pK-values for the ligand histidines of the Rieske centre were not determined experimentally, but were calculated by a combined DFT/PB approach (see Supplementary Material). The underlying DFT calculations have been shown in previous work on Rieske proteins to correctly reproduce experimental data in combination with PB-calculations [41,42]. Since in MEAD titratable groups are considered to adopt exactly two different protonation forms, the different one-proton equilibria of the Rieske centre were treated in separate MEAD-calculations, and their relative energies were then sampled by a subsequent MC analysis. Details of the treatment of the Rieske centre in the PB/MC-calculations are given in the Supplementary Material.

The following parameters were used in all PB-calculations: dielectric constants $\varepsilon=4$ for the protein and the membrane and $\varepsilon=80$ for the aqueous phase, ionic strength $I=0.1$ M for the aqueous phase and temperature $T=300$ K. Standard partial charges from the CHARMM22 parameter set [33] were used for the protein. Partial charges for other compounds (Rieske cluster, haem groups,

stigmatellin, CoQ and lipids) were derived from density functional theory calculations performed with the ADF programme suite [43]. Details of these calculations and resulting charges are given as Supplementary Material. The calculation of partial charges for the Rieske cluster [41,42] and CoQ [44] has been reported in previous publications from our group. Bondi radii [45] were used for all atoms except for hydrogen ($r_H=1.0$ Å).

From the results of the PB-calculations, the pH-dependent energy of a certain protonation and conformation state can be calculated as

$$G^{(n,k)} = \sum_i^N RT \ln 10 \cdot \left(x_i^{(n)} - x_i^{(0)}\right)\left(\text{pH} - pK_i^{\text{intr}(k)}\right)$$
$$+ \frac{1}{2}\sum_i^N \sum_j^N \left(x_i^{(n)} - x_i^{(0)}\right)\left(x_j^{(n)} - x_j^{(0)}\right)W_{i,j}^{(k)} + G_{\text{conf}}^{(k)} \qquad (1)$$

with $G^{(n,k)}$ as the energy of conformation k in protonation state n. A certain protonation state n is characterised by a protonation state vector $\overrightarrow{x}^{(n)}$ with the components $x_i^{(n)}=0$ if group i is deprotonated, and $x_i^{(n)}=1$ if group i is protonated. $x_i^{(0)}$ corresponds to the protonation form of group i in the reference protonation state of the protein, for which the intrinsic pK-values have been calculated. $pK_i^{\text{intr}(k)}$ is the intrinsic pK of group i in conformation k, which corresponds to the pK-value group i would have if all other groups were in their reference protonation form. $W_{i,j}^{(k)}$, is the interaction energy between groups i and j in conformation k, with $W_{i,j}=0$ for $i=j$. N is the total number of titratable groups, R the universal gas constant and T

the temperature. $G_{conf}^{(k)}$ accounts for the relative energies of the different conformations k considered (see above). A separate PB-calculation is performed for every conformation k.

To obtain the protonation probabilities of all groups i and the probabilities of the different conformations k as a function of pH, the states (n, k) of Eq. (1) are sampled by a Metropolis MC algorithm implemented in the programme cmct [46]. An output ensemble of low energy states is calculated for every pH (pH 0 to 14 in steps of 0.1 pH-units). At a given pH, the protonation probability $\langle x_i \rangle$(pH) of a certain group i is equivalent to the probability to find the group protonated in the MC output ensemble. In the same way, the probability of a certain conformation can be obtained from the composition of the MC output ensemble.

For every pH-step, the MC calculations consist of 500 equilibration scans and 20,000 production scans at $T = 300$ K. An MC scan consist of N MC steps, with N as total number of titratable groups. In one MC step, the protonation form of one group is changed, and the change in energy is evaluated. After every fifth MC step, the conformation of the system is changed, and the change in energy is evaluated. If the end state of a single MC step is accepted, this state is used as starting state for the next MC step. At the end of each MC production scan, the state of the system is added to the output ensemble. In double (triple) MC steps, the protonation form of two (three) groups is changed simultaneously. Double (triple) MC steps are applied to groups with an interaction energy $W_{i,j}$ larger than 2 (3) pK-units.

2.6. Correlation analysis of protonation probabilities

The electrostatic interaction among multiple titratable groups can lead to highly unusual titration behaviour of the individual groups [47,48]. To rationalise such unusual titration curves, the pairwise correlation $c_{i,j}$ (pH) of protonation probabilities is a valuable analysis tool:

$$c_{i,j}(pH) = \langle x_i x_j \rangle(pH) - \langle x_i \rangle(pH) \cdot \langle x_j \rangle(pH). \qquad (2)$$

$\langle x_i \rangle$(pH) is the probability to find group i to be protonated, irrespective of the protonation state of group j, and vice versa for $\langle x_j \rangle$(pH). In contrast, $\langle x_i x_j \rangle$(pH) is the probability to find both groups to be protonated at the same time. $c_{i,j}$(pH) takes values between -0.25 and $+0.25$. If $c_{i,j}$(pH) is large and negative, the groups i and j are anticorrelated, meaning that protonation of group i disfavours protonation of group j, and vice versa.

3. Results

3.1. Redox-linked protonation state changes in cytochrome bc_1

In order to identify redox-linked protonation state changes in cytochrome bc_1 we have calculated the titration behaviour of all titratable groups in the complex, once for the completely oxidised state, and once for the completely reduced state. In the oxidised state, all redox cofactors are oxidised and the CoQ molecules in the Q_o- and Q_i-site are in the oxidised and

deprotonated quinone form. In the reduced state, all redox cofactors are reduced and the CoQ molecules in the Q_o- and Q_i-site are in the reduced and protonated quinol form. In both redox states, the system is allowed to adopt either of the two Q_o-site conformations.

Twelve titratable groups in cytochrome bc_1 display noticeably different protonation probabilities in the completely reduced and the completely oxidised state of the system. For all other groups, the rmsd between their protonation probabilities in the reduced and oxidised state is below 0.2 for the pH-range from 0 to 14. The behaviour of most titratable groups does thus not change between the completely reduced and completely oxidised state of the system. The catalytically active dimeric cytochrome bc_1 complex from *S. cerevisiae* consists of two copies each of nine different subunits. Since equivalent titration behaviour is observed for all pairs of identical subunits in the dimeric cytochrome bc_1 complex, only the results obtained for one copy of the respective subunits are discussed, although all titratable residues in all subunits were considered in the calculations.

3.2. Conformational variability in the Q_o-site with bound CoQ

In the oxidised as well as in the reduced state of cytochrome bc_1 with CoQ in the Q_o-site, both Q_o-site conformations are populated. There are redox-linked differences in the population of the two conformations: in the oxidised complex, almost only the Glu-b conformation is populated in the physiological pH range (Fig. 4A). In the reduced complex, in contrast, also the Glu-FeS conformation is populated to a considerable degree, namely to about 30% (Fig. 4B). These results indicate that the two Q_o-site conformations observed in the crystal structures of cytochrome bc_1 from *S. cerevisiae* have sufficiently similar energies to both be populated when CoQ is bound to the Q_o-site. Furthermore, the population of the two conformations depends on pH as well as on the redox state of the complex.

In order to test our method for calculating the populations of the two different conformations, we have performed calculations on the stigmatellin-inhibited and the HDBT-inhibited complex. In these calculations, the inhibited complexes were allowed to adopt either of the two Q_o-site conformations. In agreement with the available crystallographic data, we found that the stigmatellin-inhibited complex populates exclusively
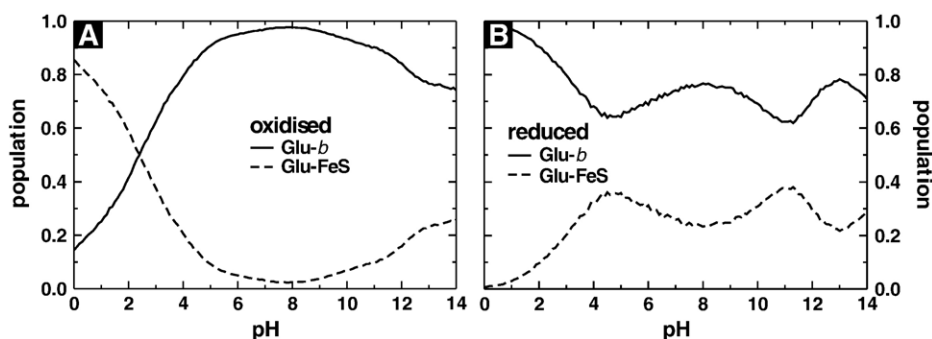

Fig. 4. Population of the different Q_o-site conformations Glu-b and Glu-FeS. (A) Completely oxidised cytochrome bc_1 with oxidised and deprotonated CoQ in the Q_o-site. (B) Completely reduced cytochrome bc_1 with reduced and protonated CoQ in the Q_o-site.

the Glu-FeS conformation, while the HDBT-inhibited complex populates exclusively the Glu-b conformation.

3.3. Redox-linked protonation state changes in the Q_o-site and cytochrome c_1

Of the twelve groups that show noticeably redox-dependent titration behaviour, five are located in the Q_o-site and one in cytochrome c_1. The titration behaviour of these residues in the completely oxidised and completely reduced complex is shown in Fig. 5. The unusual shape of the protonation probability $\langle x_i \rangle$ (pH) of E272^{CYB} in the reduced complex (Fig. 5A, dashed line) can be rationalised from its negative correlation with the protonation probability of H253^{CYB}. As outlined in more detail below, the pH-dependent correlation $c_{i,j}$(pH) is a useful tool to identify which electrostatic interactions between individual titratable residues render their titration profiles non-sigmoidal. $c_{i,j}$ (pH) takes values between +0.25 and −0.25. If $c_{i,j}$ (pH) is close to −0.25, the respective groups i and j are anticorrelated, meaning that protonation of group i disfavours protonation of group j, and vice versa. Fig. 6A displays the protonation probabilities of E272^{CYB} (dashed line), H253^{CYB} (dotted line)

and their correlation (solid line) in reduced cytochrome bc_1. The relatively large and negative correlation between these two titration curves demonstrates that deprotonation of H253^{CYB} favours protonation of E272^{CYB}. Since the protonation probability of H253^{CYB} decreases between pH 0 and pH 4, the probability to find a proton on E272^{CYB} increases in the same pH range, although the availability of protons in the solution decreases with increasing pH. In the predominant Glu-b conformation, the carboxy carbon atom of E272^{CYB} is located at a distance of 5 Å from the Nε atom of H253^{CYB} (Fig. 3). The effect of the interaction of E272^{CYB} with H253^{CYB} is amplified by an interaction with the titratable propionate A moiety of haem b_L. In the Glu-b conformation, the carboxy carbon atoms of E272^{CYB} and the propionate are separated by 7 Å (Fig. 3). Below pH 8, the protonation probabilities of the two residue show a negative correlation (Fig. 6B, solid line). Deprotonation of the propionate between pH 0 and pH 7 thus leads to an increase in the protonation probability of E272^{CYB} at low pH-values.

H141^{CYB} (Fig. 5B) and H253^{CYB} (Fig. 5C) show a slight dependence of their protonation probabilities on the redox state of the complex. The sidechain of H253^{CYB} occupies different positions in the Glu-b and Glu-FeS conformations of the Q_o-site
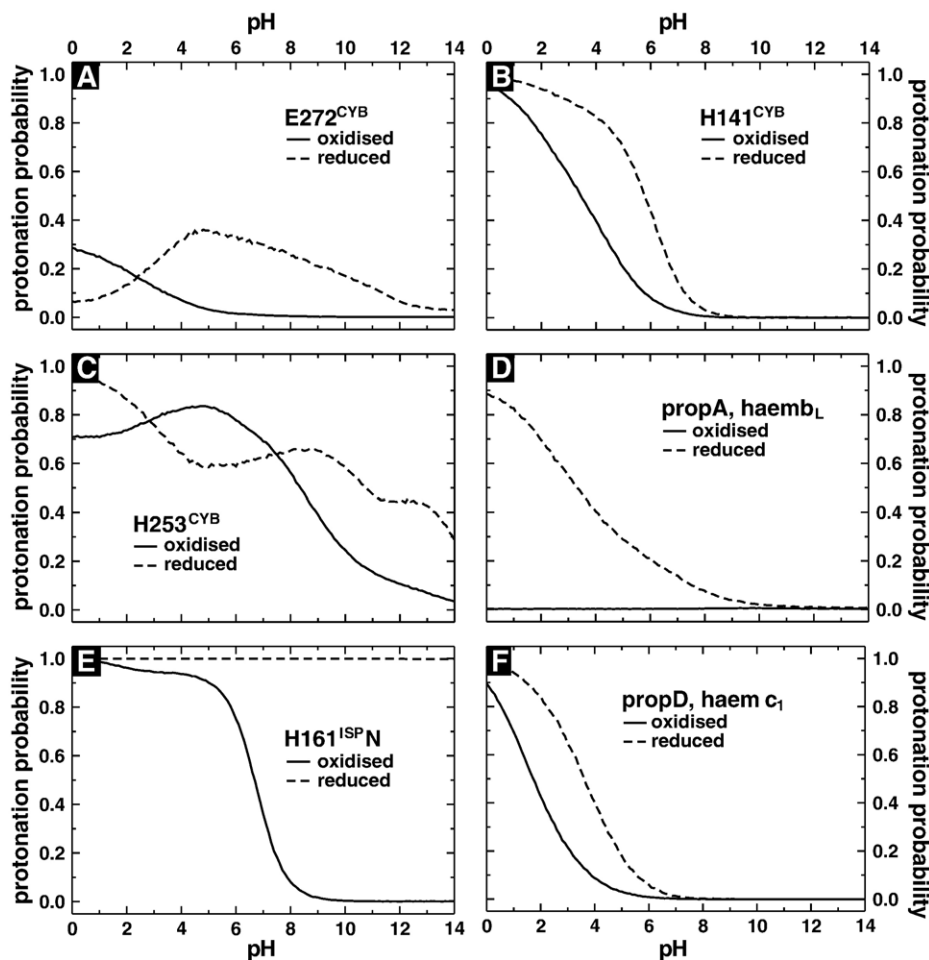

Fig. 5. Residues in the Q_o-site and the cytochrome c_1 head domain of cytochrome bc_1 that change their titration behaviour between the completely oxidised and completely reduced state. Oxidised and deprotonated or reduced and protonated CoQ is bound in the Q_o-site, respectively. H161^{ISP} is a ligand to the Rieske iron–sulphur cluster, its Nδ atom is involved in the coordination of an iron atom (Fig. 3). The second Rieske histidine ligand (H181^{ISP}) remains protonated at its Nε atom over the whole pH-range in both the oxidised and the reduced system.
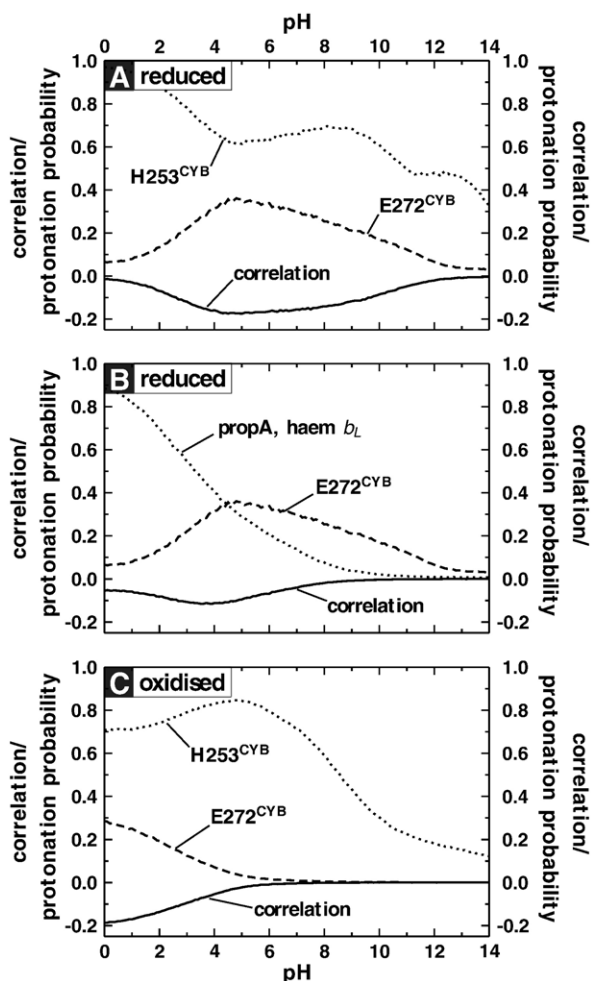
Fig. 6. Correlation between the protonation probabilities of E272^{CYB}, H253^{CYB}, and the propionate A moiety of haem b_L can rationalise the irregular shape of the titration curves of E272^{CYB} and H253^{CYB}. The pH-dependent correlation is defined as $c_{i,j}$ (pH) $= \langle x_i x_j \rangle$(pH) $- \langle x_i \rangle$(pH) $\cdot \langle x_j \rangle$(pH). In the case of e.g. the first panel, $\langle x_i \rangle$ is the protonation probability of E272^{CYB}, $\langle x_j \rangle$ is the protonation probability of H253^{CYB}, and $\langle x_i x_j \rangle$ is the probability to find both residues protonated at the same time. Each panel shows the individual protonation probability of E272^{CYB} $\langle x_i \rangle$ (dashed lines), the protonation probability of a second residue $\langle x_j \rangle$ (dotted lines), and their respective correlation (solid line) either in the oxidised or in the reduced state of the system.

(Fig. 3). The irregular shape of the titration curve of H253^{CYB} in the oxidised state can be rationalised from strong negative correlation with the protonation probability of E272^{CYB} (Fig. 6C, solid line): deprotonation of E272^{CYB} (dashed line) below pH 5 favours H253^{CYB} to remain protonated in this pH-range (dotted line). Also in fully reduced cytochrome bc_1, strong negative correlation between the protonation probabilities of H253^{CYB} and E272^{CYB} between pH 4 and pH 9 (Fig. 6A, solid line) can rationalise the plateau in the titration curve of H253^{CYB}. Deprotonation of E272^{CYB} in this pH-range stabilises the proton on H253^{CYB} and yields a higher protonation probability than would be expected for a standard sigmoidal shape.

The propionate A moiety of haem b_L (Fig. 5D) and the Rieske ligand H161^{ISP} (Fig. 5E) show a pronounced redox-dependence of their protonation probabilities. H161^{ISP} coordinates one of the Rieske iron atoms via its Nδ atom. The second Rieske histidine ligand, H181^{ISP}, remains protonated over the whole pH-range studied in both completely reduced and completely oxidised cytochrome bc_1. The titration behaviour of propionate A of haem b_L and H161^{ISP} points to a coupling between protonation of these groups and the reduction of haem b_L and the Rieske cluster, respectively.

Outside the Q_o- and Q_i-sites, the propionate D moiety of haem c_1 is the only titratable group showing a noticeable redox-linked change in titration behaviour. The weak increase in protonation probability upon conversion of the completely oxidised to the completely reduced state of the system (Fig. 5F) most likely points to a weak coupling between reduction and protonation of haem c_1.

3.4. Redox-linked protonation state changes in the UST-inhibited Q_o-site

In the UST-inhibited complex, E272^{CYB} (Fig. 7A) and H181^{ISP} (Fig. 7B) display strong redox-linked changes in their titration behaviour. Both residues have markedly higher protonation probabilities in the reduced than in the oxidised state, with reduced and oxidised UST in the active site, respectively. The second Rieske histidine ligand, H161^{ISP}, is protonated over the whole pH-range (pH 0 to 14) in both the oxidised and the reduced complex. The redox-linked change of
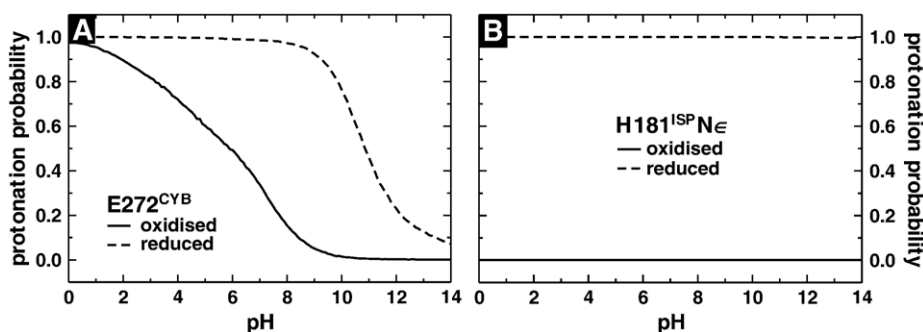

Fig. 7. Q_o-site residues with different protonation probabilities in completely oxidised and completely reduced cytochrome bc_1 with undecylstigmatellin (UST) in the Q_o-site. H181^{ISP} is a ligand to the Rieske iron–sulphur cluster, its Nδ atom coordinates one of the iron atoms (Fig. 3). The second Rieske histidine ligand (H161^{ISP}) remains protonated at its Nε atom over the whole pH-range in both the oxidised and the reduced complex with UST bound.

the protonation state of H181^{ISP} implies that a hydrogen bond between oxidised UST and the Rieske cluster can only be formed if the Rieske cluster is reduced. This observation is consistent with the experimentally detected preferential binding of stigmatellin to the reduced Rieske cluster [49,50]. In stigmatellin-inhibited cytochrome bc_1, only the Glu-FeS conformation of the Q_o-site is populated. It was thus not necessary to consider conformational variability of the UST-inhibited Q_o-site.

3.5. Redox-linked protonation state changes in the Q_i-site

In the Q_i-site, four titratable groups show noticeably redox-dependent titration behaviour. H202^{CYB} and D229^{CYB} are the two primary ligands of CoQ in the Q_i-site (Fig. 8). Both show a lower protonation probability in the oxidised than in the reduced complex (Fig. 9A and B). K228^{CYB} and K296^{CYC1} are the other two Q_i-site residues that have redox-dependent protonation probabilities. Their behaviour is less simple to describe than in the case of the direct CoQ-ligands: in both redox states of the complex, the titration curves of K228^{CYB} (Fig. 9C) and K296^{CYB} (Fig. 9D) display irregular features.

The non-standard titration curve of K228^{CYB} in oxidised cytochrome bc_1 (Fig. 9C, solid line) is due to its interaction with D229^{CYB} and K296^{CYC1}. In Fig. 10A, the protonation probabilities of K228^{CYB} (dashed line) and D229^{CYB} (dotted line) in the oxidised complex are shown together with their correlation (solid line). K228^{CYB} and D229^{CYB} display strong negative correlation between pH 6 and pH 12: as D229^{CYB} becomes deprotonated in this pH-range, the probability to find a proton on K228^{CYB} increases, even though the proton concentration in the medium decreases. The carboxy carbon atom of D229^{CYB} is located at a distance of 9 Å from the sidechain nitrogen atom of K228^{CYB} (Fig. 8). The correlation between K228^{CYB} and K296^{CYC1} in oxidised cytochrome bc_1 (Fig. 9B, solid line) is weaker than the correlation between K228^{CYB} and D229^{CYB} (Fig. 9A, solid line), but similar in shape, and K296^{CYC1} shows a titration behaviour very similar to that of D229^{CYB} (Fig. 9A and B, dotted lines). The distance between the sidechain nitrogen atoms of K228^{CYB} and K296^{CYC1} is 7 Å (Fig. 8). The interactions of K228^{CYB} with D229^{CYB} and K296^{CYC1} thus act synergistically, rendering the titration curve of K228^{CYB} highly irregular.
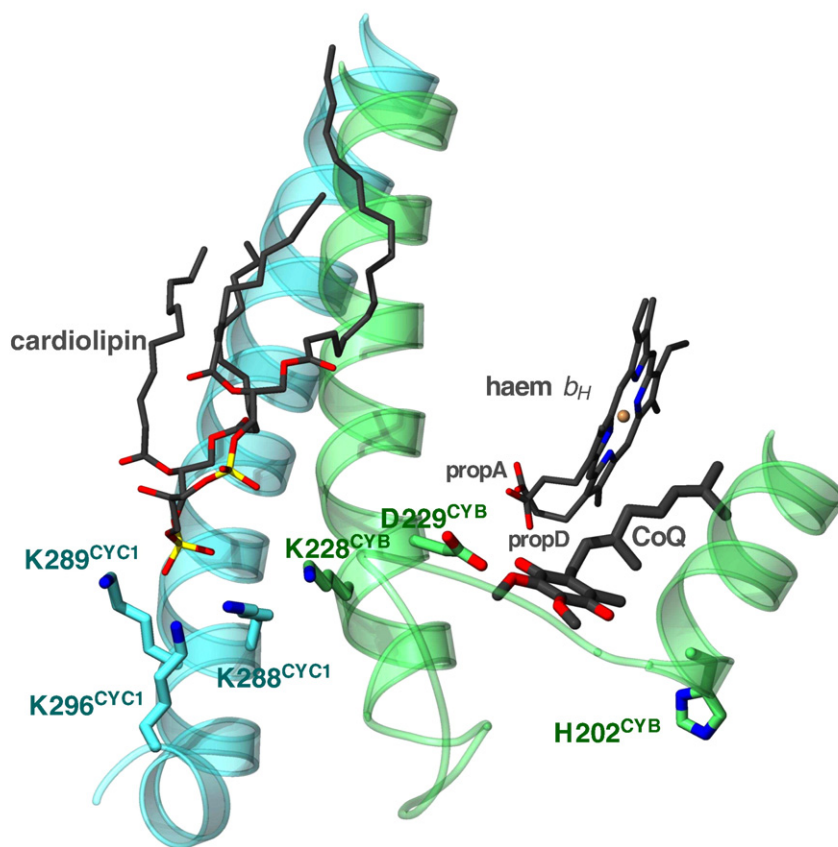

Fig. 8. The Q_i-site of cytochrome bc_1. The relevant portions of the cytochrome b subunit are shown in green, the transmembrane helix of the cytochrome c_1 subunit is shown in turquoise. Residues that undergo redox-linked protonation state changes are highlighted, together with haem b_H, the substrate CoQ, a tightly bound cardiolipin molecule, and the lysine cluster around K296^{CYC1}. K296^{CYC1} is exposed to the aqueous phase of the mitochondrial matrix, H202^{CYB} has access to the cleft between the two bundles of transmembrane helices of the dimeric complex. All other highlighted protein residues are buried within the protein. The figure was prepared from the HDBT-inhibited crystal structure of cytochrome bc_1 from S. cerevisiae [30].
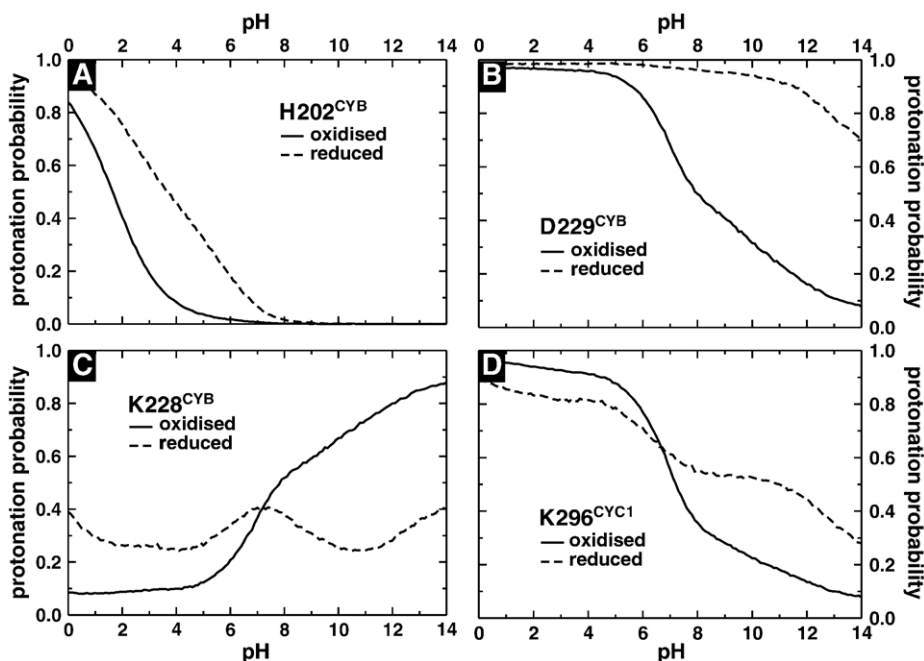
Fig. 9. Residues in the Q$_i$-site changing their titration behaviour between the completely reduced and completely oxidised state of cytochrome bc_1.
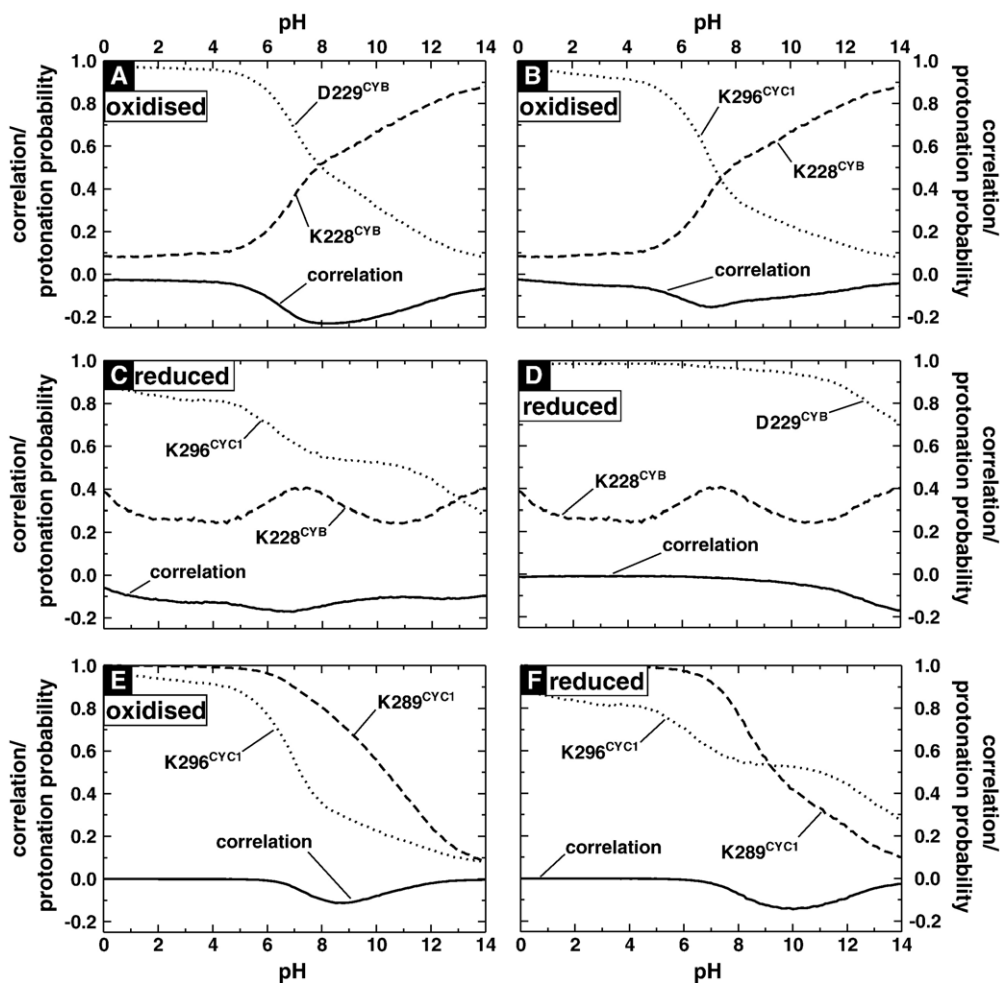
Fig. 10. Correlation of the protonation probabilities of K228^{CYB}, D229^{CYB}, K289^{CYC1} and K296^{CYC1} can explain the irregular titration curves of K228^{CYB} and K296^{CYC1} in completely reduced and completely oxidised cytochrome bc_1. Each panel shows the protonation probability of two residues (dashed and dotted lines) and their correlation $c_{i,j}$ (solid lines). If $c_{i,j}$ takes values close to -0.25 (see Eq. (2)) deprotonation of group i favours protonation of group j, and vice versa.

Also in the reduced system, the protonation probability $\langle x_i \rangle$ (pH) of K228$^{\text{CYB}}$ (Figs. 9C, 10C and D, dashed lines) has irregular features that can be explained from its correlation with the protonation probabilities of D229$^{\text{CYB}}$ and K296$^{\text{CYC1}}$. The unusual increase in protonation probability of K228$^{\text{CYB}}$ between pH 5 and pH 7 (Fig. 10C, dashed line) is due to its fairly negative correlation (Fig. 10C, solid line) with the decreasing protonation probability of K296$^{\text{CYC1}}$ (Fig. 10C, dotted line). Above pH 11, the protonation probabilities of D229$^{\text{CYB}}$ and K228$^{\text{CYB}}$ have a negative correlation (Fig. 10D, solid line): deprotonation of D229$^{\text{CYB}}$ above pH 11 (Fig. 10D, dotted line) leads to an increased protonation probability of K228$^{\text{CYB}}$ (Fig. 10D, dashed line).

The non-sigmoidal titration curve of K296$^{\text{CYC1}}$ in the oxidised system (Fig. 9D, solid line) can be explained from its interaction with K289$^{\text{CYC1}}$. The protonation probabilities of these two lysine residues have a negative correlation between pH 7 and pH 10 (Fig. 10E, solid line). As K289$^{\text{CYC1}}$ starts to deprotonate in this pH-range (Fig. 10E, dashed line), the protonation probability of K296$^{\text{CYC1}}$ (Fig. 10E, dotted line) remains higher than it would be expected for a standard sigmoidal titration curve, introducing a kink in the titration curve of K296$^{\text{CYC1}}$ at pH 8. The sidechain nitrogen atoms of K289$^{\text{CYC1}}$ and K296$^{\text{CYC1}}$ are separated by 7 Å (Fig. 8).

The titration curve of K296$^{\text{CYC1}}$ in reduced cytochrome bc_1 (Fig. 9D, dashed line) shows two flat, non-sigmoidal segments. Below pH 4, a relatively weak negative correlation between K296$^{\text{CYC1}}$ and K228$^{\text{CYB}}$ (Fig. 10C, solid line) renders the protonation probability of both residues virtually independent of pH (Fig. 9C, dashed and dotted lines). Between pH 8 and pH 12, the observed increase in protonation probability of K296$^{\text{CYC1}}$ compared to the standard sigmoidal shape is due to interaction with K289$^{\text{CYC1}}$. Similar to the situation in the oxidised system (Fig. 10E), deprotonation of K289$^{\text{CYC1}}$ in this pH-range (Fig. 10F, dashed line) shifts deprotonation of K296$^{\text{CYC1}}$ (Fig. 10F, dotted line) to higher pH values (strong negative correlation, solid line in Fig. 10F).

3.6. Effect of the membrane model on the titration behaviour of cytochrome bc_1

Since the CoQ-binding sites are known to lie at the interface of the hydrophobic membrane core and the hydrophilic lipid head group region, it is essential to consider the dielectric effect of the membrane in any attempt to calculate mechanistically relevant protonation probabilities. The positioning of the model membrane around the protein complex can be derived from the crystal structures: the dimer symmetry axis of cytochrome bc_1 corresponds to its membrane normal, and the position of the membrane along the membrane normal can be derived from the coordinates of native lipids from both monolayers of the inner mitochondrial membrane that were retained during the crystallisation procedure [29,30].

In order to characterise the effect of the model membrane on the titration behaviour of cytochrome bc_1, we have performed separate PB/MC titration calculations on the complex with and without model membrane. In both calculations cytochrome bc_1

was assumed to be fully reduced. All residues that are found to be influenced by the addition of the model membrane are located at the boundary of the membrane or in the transmembrane region of the complex. Their titration behaviour with and without model membrane is discussed in the following.

As obvious from Fig. 11, the hydrophobic membrane environment favours the neutral protonation form over the charged protonation form of all affected residues. In the hydrophobic, that means only weakly polarisable environment of the membrane, charges are destabilised in comparison to a highly polarisable aqueous solution. For example, the protonation probabilities of Y55$^{\text{ISP}}$ (Fig. 11A) and Y68$^{\text{SU9}}$ (Fig. 11B), which are equivalent to the probabilities to find them in their neutral protonation form, are increased upon addition of the membrane. Fig. 11C demonstrates that the unusually high protonation probability of D229$^{\text{CYB}}$ (also shown in Fig. 9B) is not an artefact caused by the model membrane, since this residue has a high protonation probability also in absence of the membrane (Fig. 11C, solid line).

K228$^{\text{CYB}}$ displays a highly unusual titration behaviour both with and without membrane model (Fig. 11D). The shape of the curve calculated for the complex without membrane is due to interaction with the neighbouring residues D229$^{\text{CYB}}$, K296$^{\text{CYC1}}$ and the propionate A moiety of haem b_{H} (Fig. 12). The unusual rise in protonation probability of K228$^{\text{CYB}}$ between pH 0 and pH 2 (Fig. 12A, dashed line) can be rationalised from its negative correlation (Fig. 12A, solid line) with the decreasing protonation probability of propionate A of haem b_{H} (Fig. 12A, dotted line): their negative correlation means that deprotonation of the propionate favours protonation of K228$^{\text{CYB}}$. The distance between the carboxy carbon atom of the haem propionate and the sidechain nitrogen atom of K228$^{\text{CYB}}$ is 11 Å (Fig. 8). The second and even more pronounced rise in protonation probability of K228$^{\text{CYB}}$ between pH 6 and 13 (Fig. 12B and C, dashed line) can be explained from negative correlation (Fig. 12B and C, solid lines) with the titration curves of K296$^{\text{CYC1}}$ (Fig. 12B, dotted line) and D229$^{\text{CYB}}$ (Fig. 12C, dotted line), respectively, in the pH-range from 6 to 9 and 9 to 13. K296$^{\text{CYC1}}$ starts to deprotonate at pH 6, D229$^{\text{CYB}}$ at pH 9. Correlation data rationalising the shape of the titration curve of K228$^{\text{CYB}}$ in the complex with model membrane has been discussed above and is presented in Fig. 10A to D.

K72$^{\text{ISP}}$ and E76$^{\text{ISP}}$ lie in the transmembrane region of the complex. As has been discussed in the context of the structure of cytochrome bc_1 from chicken [51], the transmembrane helix of the ISP subunit has conserved amphipathic features. In crystal structures of chicken and bovine cytochrome bc_1 [52–57], the hydrophilic patches of the ISP transmembrane helix interact with subunit 10, a small and loosely bound subunit that is not contained in the crystal structures of cytochrome bc_1 from *S. cerevisiae*. In our calculations, which are based on the crystal structures from *S. cerevisiae*, K72$^{\text{ISP}}$ and E76$^{\text{ISP}}$ are thus not involved in interaction with subunit 10, but are exposed to the hydrophobic membrane environment. The effect of the membrane model on their titration behaviour in the reduced system is shown in Fig. 11E and F (solid and dashed lines). In presence of the membrane model we observe redox-linked changes in the
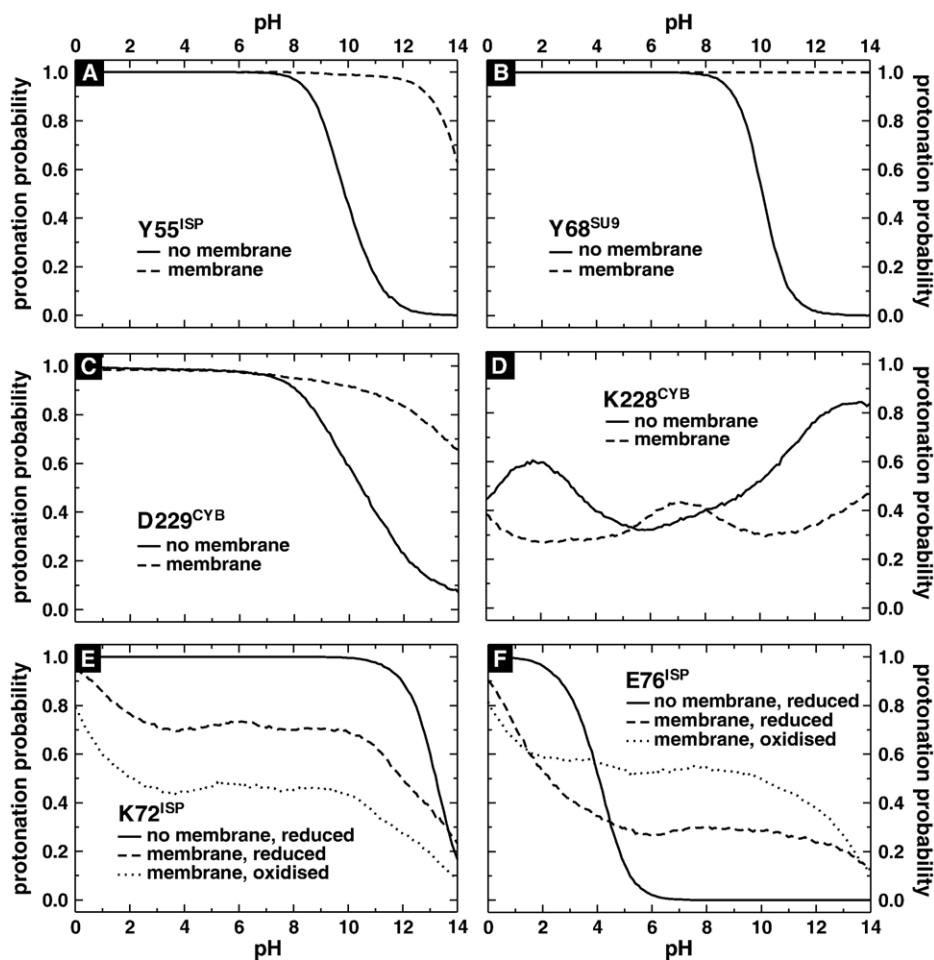
Fig. 11. Residues changing their titration behaviour upon addition of the model membrane. K72[ISP] and E76[ISP] lie in the transmembrane region of the complex, all other residues at the boundary of the model membrane. The titration behaviour of Y55[ISP] and Y68[SU9] is independent of the redox state of the system, data shown has been obtained for the fully reduced state. Redox-dependent changes in the titration behaviour of the Q_i-site residues D229[CYB] and K228[CYB] are included in Fig. 9.

titration behaviour of K72[ISP] (Fig. 11E, dashed and dotted lines) and E76[ISP] (Fig. 11F, dashed and dotted lines) that can be interpreted as a shared proton of a hydrogen bond between K72[ISP] and E76[ISP] moving slightly from E76[ISP] towards K72[ISP] upon reduction of the complex. The Nζ atom of K72[ISP] is located at a distance of 3 Å from the Oε1 atom of E76[ISP]. The protonation probabilities of K72[ISP] and E76[ISP] show a strong negative correlation when the membrane model is added. This effect is however not considered to have functional relevance in the cytochrome bc_1 complex containing subunit 10, and has therefore not been included into Fig. 5 or 9.

3.7. Proton uptake upon reduction of cytochrome bc_1

From the sum of the protonation probabilities of all titratable residues in oxidised and reduced cytochrome bc_1, the overall difference in the number of protons bound to the oxidised and reduced complex can be calculated for every pH-value. The number of protons in the reduced complex minus the number of protons in the oxidised complex is equivalent to the number of protons taken up by cytochrome bc_1 upon conversion from the oxidised to the reduced state.

Upon complete reduction of the complex, approximately three protons are taken up by each half of the dimeric complex (Fig. 13A, solid line). The uptake shows a non-linear dependence on pH. Only the protons taken up by protein residues are considered for this figure, protons of the Q/QH_2 couple are not counted. Upon conversion from the completely oxidised to the completely reduced state of the system, one electron is bound by each of the four redox cofactors (the Rieske cluster, haem b_L, haem b_H, and haem c_1). The increase in negative charge of the complex is thus compensated to about 75% by the uptake of about three protons.

4. Discussion

4.1. The conformational variability of E272[CYB] may play a role in gating of CoQ oxidation

Dutton and coworkers [19,58] have recently elaborated on an aspect of Q_o-site catalysis that has previously not attracted much attention. Since the electron transfer reactions in cytochrome bc_1 are largely reversible at least under certain experimental conditions, a control mechanism must exist that prevents
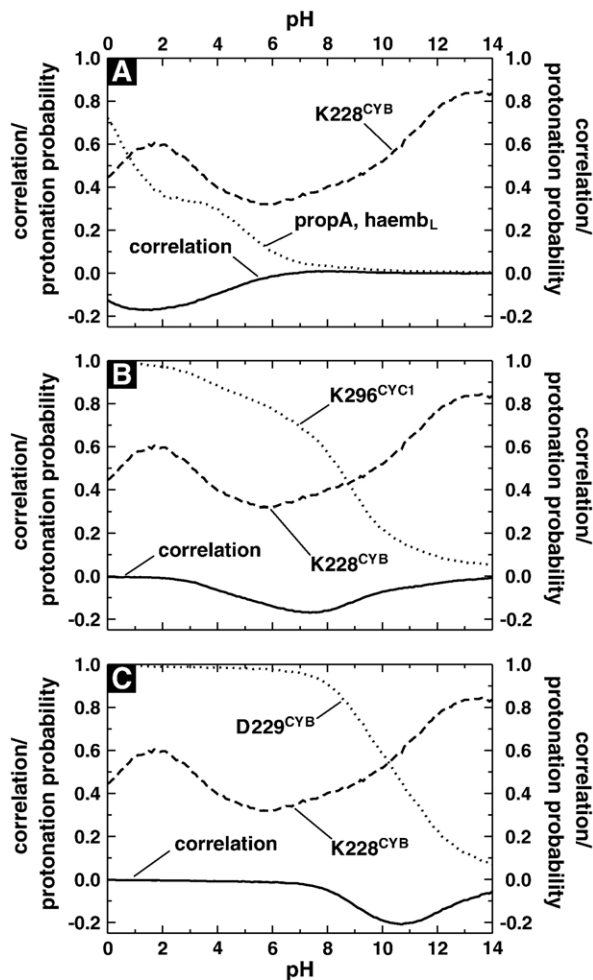
Fig. 12. Strong correlation with the protonation probabilities of D229^{CYB}, K296^{CYC1}, and the propionate A moiety of haem b_H explain the irregular titration behaviour of K228^{CYB} in the fully reduced complex without model membrane. Each panel shows the pairwise correlation $c_{i,j}$ (see Eq. (2)) between K228^{CYB} and one of these residues (solid lines), and the corresponding protonation probabilities (dashed and dotted lines).

various unproductive bypass reactions. Osyczka et al. therefore emphasised the need for a gating mechanism that allows CoQ oxidation only if the two electrons can be transferred to the two distinct electron acceptor groups. A simple scenario has been proposed [20,30] that would in fact represent such a gating mechanism: redox-dependent changes in the hydrogen-bond interactions between CoQ and the Q$_o$-site should allow binding of reduced CoQ only if both the Rieske cluster and haem b_L are oxidised. Mulkidjanian [6] introduced a similar idea where CoQ oxidation is additionally controlled by conformational changes of E272^{CYB}.

In our calculations, E272^{CYB} occupies its Glu-b position in both completely reduced and completely oxidised cytochrome bc_1 with reduced and oxidised CoQ in the Q$_o$-site, respectively (Fig. 4). In the Glu-b conformation, the carboxy group of E272^{CYB} is located at a distance of 8 Å from the closest CoQ oxygen atom and is thus unlikely to strongly interact with an uncharged CoQ (Fig. 3). The sidechain of E272^{CYB} does thus not contribute to the binding of CoQ if CoQ and the redox

cofactors of the complex are in the same redox state. In the UST-inhibited complex, where E272^{CYB} is in its Glu-FeS position, both E272^{CYB} and H181^{ISP} show redox-dependent changes in titration behaviour that are in agreement with their proposed role as primary proton acceptors (Fig. 7). When E272^{CYB} is in its Glu-b conformation, neither E272^{CYB} (Fig. 5A) nor H181^{ISP} display considerable redox-linked protonation state changes (H181^{ISP} remains protonated over the considered pH-range in both the completely oxidised and the completely reduced state). These results are consistent with the mechanism proposed by Mulkidjanian (see below and Ref. [6]).

Since the relative population of the two different conformations of the Q$_o$-site depends on pH and on the redox state of the complex (Fig. 4), it is tempting to assume that E272^{CYB} may occupy its Glu-FeS position in other combinations of the redox states of CoQ and the protein cofactors. In the Glu-FeS position, the sidechain of E272^{CYB} is most likely a primary ligand to CoQ, since it directly interacts with the inhibitor stigmatellin in the respective crystal structures [4,28,29,56,57,59,60]. Our results for the completely reduced and completely oxidised complex still allow for the conformational variability of E272^{CYB} being a mechanistic basis for the gating of CoQ oxidation in the Q$_o$-site.

The following scenario for the gating of CoQ oxidation in the Q$_o$-site by means of a change of its conformation and protonation is thus consistent with our data (compare Ref. [6]): if reduced and protonated CoQ enters into the Q$_o$-site of reduced cytochrome bc_1 it cannot bind strongly because the sidechain of E272^{CYB} is in its Glu-b position and pointing away from the binding site. Also the Rieske ligand H181^{ISP} is protonated and cannot serve as a hydrogen bond acceptor. In contrast, if reduced and protonated CoQ binds to oxidised cytochrome bc_1 (that is not the oxidised and deprotonated form present in our calculations on the oxidised complex), E272^{CYB} may occupy its Glu-FeS position. H181^{ISP} and E272^{CYB} would then be deprotonated and ready to bind the quinol by each accepting a hydrogen bond. Both H181^{ISP} and E272^{CYB} would in this situation show redox-linked changes in their protonation probabilities, which makes them likely candidates for the uptake of one proton each upon electron transfer from CoQ to the Rieske cluster and haem b_L.

4.2. Coupling between reduction and protonation of haem b_L and the Rieske cluster

The redox-linked change in the protonation probability of the propionate A of haem b_L (Fig. 5D) points to a coupling between the reduction and protonation of this cofactor. Such an effect would support the parallel movement of an electron and a proton from reduced CoQ towards haem b_L [9,28]. The movement of compensating charges may be energetically favourable for electron transfer from CoQ to haem b_L. Electron transfer within cytochrome b has in fact been reported to be electrogenically silent even up to the stage of CoQ reduction in the Q$_i$-site [6].

As obvious from the data presented in Fig. 5E, the Rieske histidine ligand H161^{ISP} shows a strong dependence of its protonation probability on the redox state of the system.
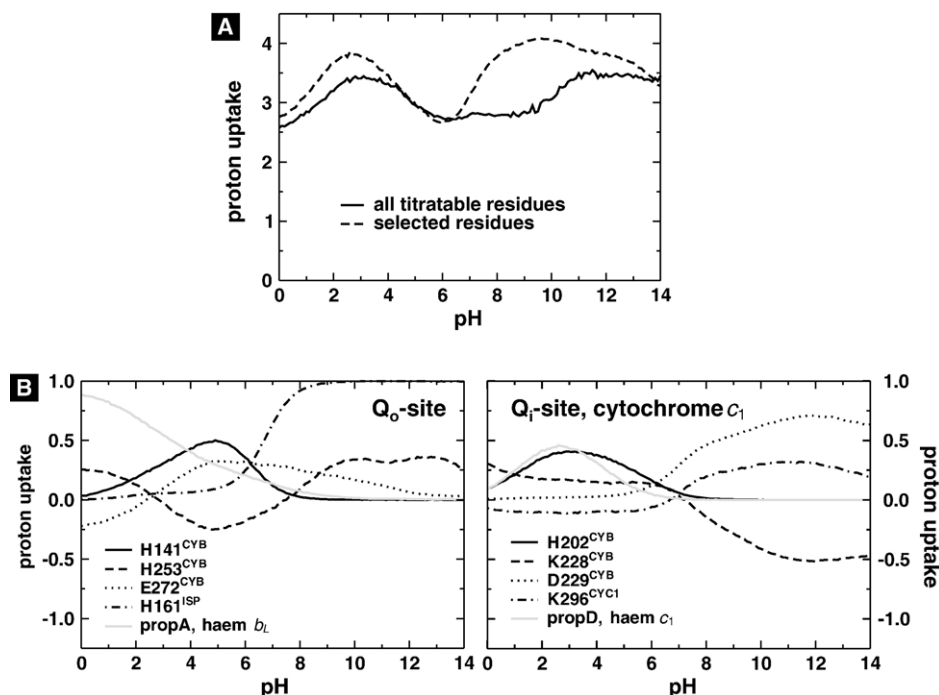
Fig. 13. Proton uptake upon reduction of cytochrome bc_1. (A) The total number of protons taken up by one half of the dimeric system is shown as solid line. The contributions of all titratable residues have been considered to calculate this quantity. The dashed line shows the number of protons taken up by only a subset of the titratable residues (H141[CYB], H253[CYB], E272[CYB], H161[ISP], propionate A of haem b_L, H202[CYB], K228[CYB], D229[CYB], K296[CYC1] and propionate D of haem c_1). (B) Contributions of the individual residues that add up to the dashed line in panel A.

Coupling between reduction and protonation of the Rieske cluster in isolated ISP fragments has been reported [8,9,15,28,61], and protonation state changes of the Rieske cluster have also been observed in FTIR experiments in the context of the cytochrome bc_1 complex [27]. The latter results are largely equivalent to our data, but in the experiments the Q_o-site is most likely empty, and the localisation of the mobile ISP head domain at the Q_o-site interface with cytochrome b is therefore not assured [4,53,62]. Our calculations now provide evidence that the coupling between protonation and reduction of the Rieske cluster plays a role also in the structural context of the Q_o-site.

4.3. Primary proton donor groups and proton uptake towards the Q_i-site

H202[CYB] and D229[CYB] are primary ligands of CoQ in the Q_i-site (Fig. 8). Our results for their protonation probabilities are consistent with the role of these residues as primary proton donor groups during CoQ reduction in the Q_i-site: when haem b_H gets oxidised via electron transfer to CoQ in the Q_i-site, the protonation probabilities of H202[CYB] and D229[CYB] are likely to decrease as observed in our calculations (Fig. 9A and B). Protons from these two residues could then easily be transferred to the CoQ molecule in the Q_i-site.

The highly irregular titration behaviour of K228[CYB] and K296[CYC1], together with their correlation with D229[CYB] and K289[CYC1], respectively, shows that the titratable residues of the Q_i-site form a network of strongly interacting groups. It is important to quantify the effect of electrostatic interaction

between these titratable residues to assess their role in proton uptake to the Q_i-site. Non-standard titration curves of individual titratable groups in proteins are in general due to strong electrostatic interaction with at least one other titratable group [48], meaning that the pairwise interaction energy $W_{i,j}$ (Eq. (1)) takes a large value. However, since the interaction energy $W_{i,j}$ is a pH-independent quantity, the correlation $c_{i,j}$ (pH) between the titration curves $\langle x_i\rangle$(pH) and $\langle x_j\rangle$(pH) of two interacting groups i and j is a more significant and intuitive tool to rationalise the non-standard titration curves of interacting groups: strongly interacting groups that titrate in the same pH-range are likely to show correlation of their protonation probabilities, but the correlation may vary with pH. The correlation $c_{i,j}$ (pH) (Eq. (2)) is a unitless number that takes values between -0.25 and $+0.25$. A relatively large and negative value of $c_{i,j}$ (pH) means that protonation of group i disfavours protonation of group j, and vice versa.

Because of the strong correlation of the protonation probabilities of K228[CYB], D229[CYB] and K296[CYC1] we propose that these residues form a concerted device for proton uptake to the Q_i-site. While the putative primary proton donor group D229[CYB] is buried within the protein, K296[CYC1] is exposed to the aqueous phase of the mitochondrial matrix. K228[CYB] is located between K296[CYC1] and D229[CYB] (Fig. 8). Protons from the mitochondrial matrix might therefore reach the Q_i-site via K296[CYC1] and K228[CYB]. K228[CYB] and K296[CYC1] are conserved over a wide range of species. The unusual, non-sigmoidal titration curves of K228[CYB] show that the protonation state of this residue is highly ambivalent, which makes it a likely residue to be involved in proton transfer. Besides, K228[CYB] is part of a

cluster of four conserved lysine residues (K228^{CYB}, K288^{CYC1}, K289^{CYC1} and K296^{CYC1}; Fig. 8) that also display relatively strong correlations of their protonation probabilities. This lysine cluster may act as a proton sink to increase the probability of protons reaching the Q$_i$-site.

Previous investigations of the structure of the Q$_i$-site of cytochrome bc_1 from *S. cerevisiae* have proposed different possibilities of proton uptake towards D229^{CYB} [9,29]. Lange et al. [29] have discussed the so-called CDL/K-pathway as one possible route of proton uptake towards D229^{CYB}. They proposed a role in proton uptake for the tightly bound cardiolipin molecule (CDL) located close to K228^{CYB} (Fig. 8). Our calculations indicate that CDL is not directly involved in proton uptake since both of its phosphate moieties remain deprotonated between pH 0 and pH 14 in both redox states of the complex. Instead, K296^{CYB} and the surrounding lysine residues may take the role of the primary proton uptake group. The cardiolipin molecule can still have an essential role in stabilising protons in this lysine cluster: the protonation probabilities of K288^{CYC1} (Fig. 14A) and K289^{CYC1} (Fig. 14B) drop dramatically if the CDL molecule is omitted from the calculations. Other residues are not affected substantially by the presence or absence of CDL.

4.4. Account of the membrane model

The need to include a membrane model in PB-calculations on cytochrome bc_1 is immediately evident from the location of the CoQ-binding sites at the interface of the hydrophobic membrane core and the hydrophilic lipid head group region of the mitochondrial membrane. We employ a straight-forward model of the membrane that as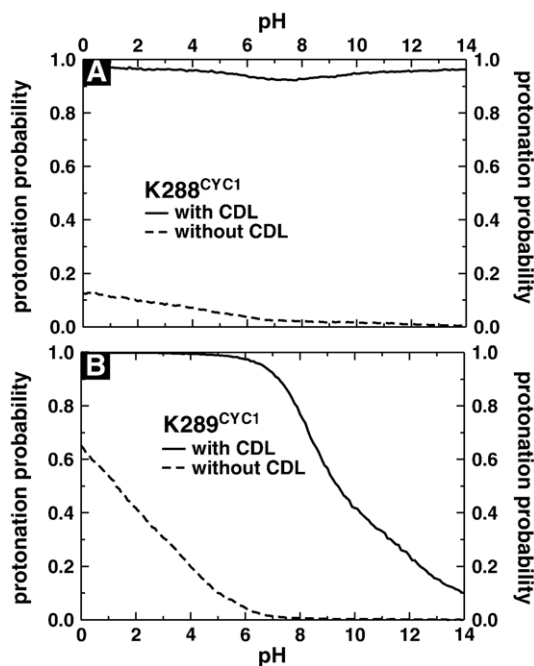sumes a low dielectric constant for the membrane core (the same as for the protein) and a high dielectric constant for the lipid head group region (the same as for the aqueous phase). Our model has the advantage to be applicable to all three-dimensional arrangements of protein/membrane and protein/water interfaces. Future approaches to PB-calculations on membrane proteins will ideally combine this feature with a more accurate treatment of the headgroup region. The thorough test calculations on the effect of the model membrane show that it yields reasonable results since the titration behaviour of all affected residues is changed towards a stabilisation of the uncharged forms. At the same time, the dominant features in the titration curves of the relevant Q$_i$-site residues D229^{CYB} (high protonation probability even at high pH) and K228^{CYB} (intermediate protonation probability that is only weakly pH-dependent) are evident also in absence of the membrane model. We therefore conclude that the unusual titration behaviour of these residues is not an artefact of the calculation setup but is relevant to the understanding of the catalytic mechanism of cytochrome bc_1.

4.5. Comparison of calculated protonation probabilities and FTIR data

Several FTIR experiments have been performed in recent years to identify redox-dependent protonation state changes in cytochrome bc_1 [22–27]. In these studies, the completely reduced system is converted into the completely oxidised system, and redox-dependent FTIR difference spectra are recorded during this transition.

For the Q$_o$-site, direct comparison of FTIR data and calculated protonation probabilities is possible for the results obtained with an UST-inhibited Q$_o$-site, since in this case the conditions of experiment and calculations are largely equivalent. Upon reduction of haem b_L, Ritter et al. [25] observe a change in a signal assigned to a propionate group. In our calculations with UST none of the propionate groups of cytochrome bc_1 displays noticeable redox-linked changes in its protonation probability. Since the discrimination of FTIR signals from propionate and sidechain carboxy groups is often not trivial, we propose that the observed signal may originate from the marked redox-dependence of the protonation probability of E272^{CYB} (Fig. 7). In the UST-inhibited complex the sidechain of E272^{CYB} is located at a distance of only 7.7 Å from the haem porphyrin ring system which makes it a likely candidate for coupling to the reduction of haem b_L.

Apart from the work on UST-inhibited cytochrome bc_1, most of the available FTIR data has been obtained with an empty Q$_o$-site. If the Q$_o$-site is empty, the ISP head domain will occupy many different positions, as indicated by an early crystallographic study of uninhibited cytochrome bc_1 that could not resolve the ISP head domain [52]. It can be assumed that the mobile and consequently well solvated ISP head domain will in this situation have little effect on the electrostatics of the rest of the complex. To mimic the experimental conditions of the FTIR studies of uninhibited cytochrome bc_1 we have therefore characterised the titration behaviour of reduced cytochrome bc_1 with an empty Q$_o$-site in the Glu-b conformation and

Fig. 14. Effect of cardiolipin (CDL) on the titration behaviour of residues located close to the Q$_i$-site of cytochrome bc_1. Results shown were obtained for completely reduced cytochrome bc_1, neither of the two residues shows redox-dependent titration behaviour.

without the ISP head domain. Our results for this scenario are virtually identical to the results for the complete system with CoQ in the Q_o-site. The results presented above can therefore reasonably be compared to the available FTIR data also without UST in the Q_o-site, keeping in mind that we can however not easily decide on the conformation of the cytochrome b part of the empty Q_o-site. More detailed structural information is required to asses this question in PB/MC titration calculations.

Baymann et al. [22] observe the protonation of a carboxylic group to be coupled to the reduction of haem b_L, and propose $E272^{CYB}$ as a likely candidate responsible for this effect. From our calculations with CoQ in the Q_o-site, $E272^{CYB}$ shows only a slightly higher protonation probability in the completely reduced compared to the completely oxidised complex. Since the Q_o-site is however empty in the experiments, $E272^{CYB}$ may occupy its Glu-FeS position. For this scenario, we expect from our data a marked increase in the protonation probability of $E272^{CYB}$ upon reduction of the protein complex, which is in agreement with the experimental data. Ritter et al. [23] observe changes in a signal from a propionate group upon reduction of haem c_1, which fits with the redox-linked changes in titration behaviour of the propionate D moiety of haem c_1 in our calculations. Iwaki et al. [27] report redox-linked changes in the protonation state of the Rieske ligand histidines that are in agreement with our results. Ritter et al. [23,25] report an unexpected protonation of a carboxylic residue upon oxidation of the complex. In our calculation, we cannot identify a residue undergoing an equivalent redox-linked change in protonation state. However, Baymann et al. [22] observe the protonation of a carboxylic group upon reduction of haem b_H. Our results fit well with these latter data: we observe the protonation of $D229^{CYB}$ to be coupled to reduction of cytochrome bc_1 (Fig. 9B). The specific coupling between haem b_H and $D229^{CYB}$ can be concluded from their close spatial proximity (Fig. 8).

4.6. Proton uptake upon reduction of cytochrome bc_1

The shape of the proton uptake curve vs. pH (relatively high values at pH 3 and pH>10, Fig. 13A, solid line) can be rationalised by a simple statistical consideration. In a system with multiple titratable groups, the titration behaviour of the individual groups can differ considerably from their behaviour as isolated group in aqueous solution. However, the majority of all titratable groups will be solvent exposed and still titrate in a pH-range around their solution pK-values. Thus, at pH-values around 4, the majority of the carboxylic residues will titrate. At pH-values above 10, the majority of the arginine and lysine residues will titrate. In the intermediate pH-region, only the histidine residues are likely to titrate, and their number is much lower than the number of carboxylic, arginine and lysine residues (43 histidines vs. 192 carboxylic residues and 203 arginine and lysine residues in each half of the dimeric complex). If many residues are likely to titrate at a certain pH-value, small redox-linked changes in the protonation probabilities of some of these residues will add up to a considerable value. Such relatively high values of the sum of redox-linked changes in protonation probabilities correspond to

the high values for proton uptake upon reduction at pH 4 (carboxylic residues) and above pH 10 (arginine and lysine residues). The relative frequency of the different types of titratable residues can thus roughly rationalise the shape of the proton uptake curve.

In our analysis of the redox-linked changes in titration behaviour of cytochrome bc_1 we focus on those residues that have an rmsd between their titration curves in the oxidised and reduced state (over the pH-range from 0 to 14) that exceeds a threshold value of 0.2. Based on this selection criterion, we discuss the titration behaviour of the following residues: propionate D of haem c_1, the Q_o-site residues $H141^{CYB}$, $H253^{CYB}$, $E272^{CYB}$, $H161^{ISP}$ and propionate A of haem b_L, and the Q_i-site residues $H202^{CYB}$, $K228^{CYB}$, $D229^{CYB}$ and $K296^{CYC1}$. The proton uptake that can be attributed to this set of ten groups is shown in Fig. 13A (dashed line), and the contribution of the individual residues is shown in Fig. 13B. The total proton uptake of the altogether 554 titratable residues in each half of the dimeric complex has a slightly different pH-dependence than the uptake by the set of selected residues, especially in the pH range from 7 to 12. Therefore, also residues that undergo only subtle redox-linked changes in their titration behaviour and are thus not discussed explicitly, make a contribution to the total uptake of protons upon reduction of cytochrome bc_1. If one considers however that the set of selected residues comprises less than 2% of the total number of titratable residues in the system, the difference between the two proton uptake curves is small. The residues that are most important for redox-linked protonation state changes in cytochrome bc_1 have thus been discussed above.

5. Conclusions

By performing Poisson–Boltzmann/Monte Carlo titration calculations, we have obtained protonation probabilities for completely oxidised cytochrome bc_1 with oxidised and deprotonated CoQ or undecylstigmatellin in the Q_o-site, and completely reduced cytochrome bc_1 with reduced and protonated CoQ or UST bound. We could identify a small number of residues in the protein complex which show different titration behaviour in the completely reduced and the completely oxidised state of cytochrome bc_1. The obtained results are largely consistent with the available FTIR data [22–27]. In addition to the protonation probabilities, we have calculated the population of two different conformations of the Q_o-site as a function of ambient pH and of the redox state of the complex. $E272^{CYB}$ has been shown to occupy different positions in the Q_o-site: in stigmatellin-inhibited cytochrome bc_1 the sidechain of $E272^{CYB}$ binds stigmatellin together with the Rieske cluster (conformation Glu-FeS), while in the HDBT-inhibited complex it points away from the inhibitor and towards haem b_L (conformation Glu-b). Our calculations indicate that in presence of CoQ modelled into the Q_o-site both the completely reduced and the completely oxidised complex populate primarily the Glu-b conformation. However, the relative population of the two conformations depends on pH as well as on the redox state of the complex. In the completely reduced state of cytochrome

bc_1 also the Glu-FeS conformation of the Q_o-site is considerably populated in the physiological pH range. Our data thus indicate that the two crystallographically observed conformations of the Q_o-site can be populated in the uninhibited complex, and that the corresponding conformational change may well play a role during turnover of the Q_o-site.

The calculated protonation probabilities and populations of the different Q_o-site conformations have mechanistic implications for Q_o-site catalysis. We have shown that coupling between the reduction and protonation of the Rieske cluster plays a role also in the context of the Q_o-site with bound CoQ. The redox-linked change in the protonation probability of propionate A of haem b_L supports a proposed parallel movement of an electron and a proton from CoQ to haem b_L. The observed redox-dependence of the population of the different Q_o-site conformations and of the protonation probability of E272^{CYB} imply, that a change of the conformation and protonation of E272^{CYB} will most likely be involved in the CoQ oxidation reaction. The conformational transition of E272^{CYB} and resulting changes in the protonation pattern of the Q_o-site may be the basis of a redox-dependent gating of CoQ binding to the protein complex: if CoQ and the redox cofactors of cytochrome bc_1 are in the same redox state, CoQ cannot bind strongly since E272^{CYB} is in its Glu-b position and points away from the binding site. In this situation, neither of the two postulated primary proton acceptor groups of the CoQ oxidation reaction (E272^{CYB} and the Rieske ligand H181^{ISP}) display redox-dependent protonation probabilities that would fit with the proposed catalytic function.

If H161^{ISP} undergoes protonation upon reduction, if E272^{CYB} is in its Glu-b conformation, only the second Rieske histidine ligand, H161^{ISP} undergoes protonation upon reduction. However, E272^{CYB} may occupy its Glu-FeS conformation when reduced and protonated CoQ binds to oxidised cytochrome bc_1. The conformational change of E272^{CYB} induces changes in the protonation pattern of the Rieske cluster and the E272^{CYB} sidechain, so that both E272^{CYB} and H181^{ISP} are then likely proton acceptor groups. In the future, we will test the implications of our present work by calculating protonation probabilities for combinations of redox states of CoQ and the protein complex that are possible intermediates of cytochrome bc_1 turnover.

Concerning the Q_i-site, our results are in agreement with the role of H202^{CYB} and D229^{CYB} as primary proton donor groups during the reduction of quinone. Based on calculated redox-linked changes in protonation probabilities, strong correlation of protonation probabilities, and an analysis of the solvent-exposure of contributing residues, we propose that residues K296^{CYC1}, K288^{CYB} and D229^{CYB} form a concerted device for proton uptake towards the Q_i-site. The negatively charged headgroup of the cardiolipin molecule located close to the Q_i-site stabilises protons in a cluster of lysine residues around K296^{CYC1}.

To the best of our knowledge, the present paper is the first report of a quantitative theoretical investigation of the titration behaviour of a system as large as cytochrome bc_1, based on physical principles and structural data at atomic detail. We present here calculations of protonation probabilities that have been performed in order to mimic the experimental setup of recently published FTIR experiments. Our results are in agreement with experimental data and aid in the understanding of the molecular mechanism of cytochrome bc_1.

Acknowledgements

Appendix A. Supplementary data

Supplementary data associated with this article can be found, in the online version, at doi:10.1016/j.bbabio.2007.01.016.

References

[1] P. Mitchell, Possible molecular mechanism of the protonmotive function of cytochrome systems, J. Theor. Biol. 62 (1976) 327–367.

[2] P.B. Garland, R.A. Clegg, D.H. Boxer, J.A. Downie, B.A. Haddock, Proton-translocating nitrate reductase of *Escherichia coli*. In: E. Quagliariello, S. Papa, F. Palmieri, E.C. Slater, N. Siliprandi (Eds.), Electron transfer chains and oxidative phosphorylation, Elsevier/North Holland, 1975, pp. 351–358.

[3] A.R. Crofts, S.W. Meinhardt, K.R. Jones, M. Snozzi, The role of the quinone pool in the cyclic electron transfer chain of *Rhodopseudomonas sphaeroides*, Biochim. Biophys. Acta 723 (1983) 202–218.

[4] Z. Zhang, L. Huang, V.M. Shulmeister, Y.-I. Chi, L.L. Lim, L.-W. Hung, A.R. Crofts, E.A. Berry, S.-H. Kim, Electron transfer by domain movement in cytochrome bc_1, Nature 392 (1998) 677–684.

[5] A.R. Crofts, The cytochrome bc_1 complex: function in the context of structure, Annu. Rev. Physiol. 66 (2004) 689–733.

[6] A.Y. Mulkidjanian, Ubiquinol oxidation in the cytochrome $bc1$ complex: reaction mechanism and prevention of short-circuiting, Biochim. Biophys. Acta 1709 (2005) 5–34.

[7] E.A. Berry, Z. Zhang, L.-S. Huang, S.-H. Kim, Structures of quinone-binding sites in bc complexes: functional implications, Biochem. Soc. Trans. 27 (1999) 565–572.

[8] A.R. Crofts, S. Hong, N. Ugulava, B. Barquera, R. Gennis, M. Guergova-Kuras, E.A. Berry, Pathways for proton release during ubihydroquinone oxidation by the bc_1 complex, Proc. Natl. Acad. Sci. U. S. A. 96 (1999) 10021–10026.

[9] C. Hunte, H. Palsdottir, B.L. Trumpower, Protonmotive pathways and mechanisms in the protonmotive cytochrome bc_1 complex, FEBS Lett. 545 (2003) 39–46.

[10] T. Wenz, P. Hellwig, F. MacMillan, B. Meunier, C. Hunte, Probing the role of E272 in quinol oxidation of mitochondrial complex III, Biochemistry 45 (2006) 9042–9052.

[11] T. Wenz, R. Covian, P. Hellwig, F. MacMillan, B. Meunier, B.L. Trumpower, C. Hunte, Mutational analysis of cytochrome b at the ubiquinol oxidation site of yeast complex III, J. Biol. Chem. 282 (2007) 3977–3988.

[12] U. Brandt, Control of ubiquinol oxidation at center P (Qo) of the cytochrome bc_1 complex, J. Bioenerg. Biomembr. 31 (1999) 243–250.

[13] S. Hong, N. Ugulava, M. Guergova-Kuras, A.R. Crofts, The energy landscape for ubihydroquinone oxidation at the Q_o site of the bc_1 complex in *Rhodobacter sphaeroides*, J. Biol. Chem. 274 (1999) 33931–33944.

[14] A.R. Crofts, M. Guergova-Kuras, R. Kuras, N. Ugulava, J. Li, S. Hong, Proton-coupled electron transfer at the Q_o site: what type of mechanism can account for the high activation barrier? Biochim. Biophys. Acta 1459 (2000) 456–466.

[15] T.A. Link, The role of the 'Rieske' iron sulfur protein in the hydroquinone oxidation (QP) site of cytochrome bc_1 complex. The proton gated affinity change mechanism, FEBS Lett. 412 (1997) 257–264.

[16] S. Jünemann, P. Heathcote, P.R. Rich, On the mechanism of quinol oxidation in the bc_1 complex, J. Biol. Chem. 273 (1998) 21603–21607.

[17] U. Brandt, The chemistry and mechanics of ubihydroquinone oxidation at center P (Q_o) of the cytochrome bc_1 complex, Biochim. Biophys. Acta 1365 (1998) 261–268.

[18] J. Yan, G. Kurisu, W.A. Cramer, Intraprotein transfer of the quinone analogue inhibitor 2,5-dibromo-3-methyl-6-isopropyl-p-benzoquinone in the cytochrome b_6f complex, Proc. Natl. Acad. Sci. U. S. A. 103 (2006) 69–74.

[19] A. Osyczka, C.C. Moser, F. Daldal, P.L. Dutton, Reversible redox energy coupling in electron transfer chains, Nature 427 (2004) 607–612.

[20] P.R. Rich, The quinone chemistry of bc complexes, Biochim. Biophys. Acta 1658 (2004) 165–171.

[21] J.L. Cape, J.R. Strahan, M.J. Lenaeus, B.A. Yuknis, T.T. Le, J.N. Shepherd, M.K. Bowman, D.M. Kramer, The respiratory substrate rhodoquinol induces Q-cycle bypass reactions in the yeast cytochrome bc_1 complex: mechanistic and physiological implications, J. Biol. Chem. 280 (2005) 34654–34660.

[22] F. Baymann, D.E. Robertson, P.L. Dutton, W. Mäntele, Electrochemical and spectroscopic investigations on the cytochrome bc_1 complex from Rhodobacter capsulatus, Biochemistry 38 (1999) 13188–13199.

[23] M. Ritter, O. Anderka, B. Ludwig, W. Mäntele, P. Hellwig, Electrochemical and FTIR spectroscopic characterization of the cytochrome bc_1 complex from Paracoccus denitrificans: evidence for protonation reactions coupled to quinone binding, Biochemistry 42 (2003) 12391–12399.

[24] M. Iwaki, L. Giotta, A.O. Akinsiku, H. Schägger, N. Fisher, J. Breton, P.R. Rich, Redox-induced transitions in bovine cytochrome bc_1 complex studied by perfusion-induced ATR-FTIR spectroscopy, Biochemistry 42 (2003) 11109–11119.

[25] M. Ritter, H. Palsdottir, M. Abe, W. Mäntele, C. Hunte, H. Mayoshi, P. Hellwig, Direct evidence for the interaction of stigmatellin with a protonated acidic group in the bc_1 complex from Saccharomyces cerevisiae as monitored by FTIR difference spectroscopy and ^{13}C specific labeling, Biochemistry 43 (2004) 8439–8446.

[26] M. Iwaki, A. Osyczka, C.C. Moser, P.L. Dutton, P.R. Rich, ATR-FTIR spectroscopy studies of iron-sulfur protein and cytochrome c_1 in the Rhodobacter capsulatus cytochrome bc_1 complex, Biochemistry 43 (2004) 8486–9477.

[27] M. Iwaki, G. Yakovlev, J. Hirst, A. Osyczka, P.L. Dutton, D. Marshall, P.R. Rich, Direct observation of redox-linked histidine protonation changes in the iron–sulfur protein of the cytochrome bc1 complex by ATR-FTIR spectroscopy, Biochemistry 44 (2005) 4230–4237.

[28] C. Hunte, J. Koepke, C. Lange, T. Roßmanith, H. Michel, Structure at 2.3 Å of the cytochrome bc_1 complex from the yeast Saccharomyces cerevisiae co-crystallized with an antibody Fv fragment, Structure 8 (2000) 669–684.

[29] C. Lange, J.H. Nett, B.L. Trumpower, C. Hunte, Specific roles of protein–phospholipid interactions in the yeast cytochrome bc_1 complex structure, EMBO J. 20 (2001) 6591–6600.

[30] H. Palsdottir, C.G. Lojero, B.L. Trumpower, C. Hunte, Structure of the yeast cytochrome bc_1 with a hydroxyquinone anion Q_o site inhibitor bound, J. Biol. Chem. 278 (2003) 31303–31311.

[31] H. Palsdottir, C. Hunte, Lipids in membrane protein structures, Biochim. Biophys. Acta 1666 (2004) 2–18.

[32] R. Covian, B.L. Trumpower, Regulatory interactions between ubiquinol oxidation and ubiquinone reduction sites in the dimeric cytochrome bc_1 complex, J. Biol. Chem. 281 (2006) 30925–30932.

[33] A.D. MacKerell, D. Bashford, M. Bellott, R.L. Dunbrack jr., J.D. Evanseck, M.J. Field, S. Fischer, J. Gao, H. Guo, S. Ha, D. Joseph-McCarthy, L. Kuchnir, K. Kuczera, F.T.K. Lau, C. Mattos, S. Michnick, T. Ngo, D.T. Nguyen, B. Prodhom, W.E. Reiher, B. Roux, M. Schlenkrich, J.C. Smith, R. Stote, J. Straub, M. Watanabe, J. Wiorkiewicz-Kuczera, D. Yin, M. Karplus, All-atom empirical potential for molecular modeling and dynamics studies of proteins, J. Phys. Chem., B 102 (1998) 3586–3616.

[34] C.R.D. Lancaster, H. Michel, The coupling of light-induced electron transfer and proton uptake as derived from crystal structures of reaction centres from Rhodopseudomonas viridis modified at the binding site of the secondary quinone, QB, Structure 5 (1997) 1339–1359.

[35] A.R. Crofts, B. Barquera, R.B. Gennis, R. Kuras, M. Guergova-Kuras, E.A. Berry, Mechanism of ubiquinol oxidation by the bc_1 complex: different domains of the quinol binding pocket and their role in the mechanism and binding of inhibitors, Biochemistry 38 (1999) 15807–15826.

[36] N. Calimet, G.M. Ullmann, The effect of a transmembrane pH gradient on protonation probabilities of bacteriorhodopsin, J. Mol. Biol. 339 (2004) 571–589.

[37] G.M. Ullmann, E.-W. Knapp, Electrostatic models for computing protonation and redox equilibria in proteins, Eur. Biophys. J. 28 (1999) 533–551.

[38] M.R. Gunner, J. Mao, Y. Song, J. Kim, Factors influencing the energetics of electron and proton transfers in proteins. What can be learned from calculations, Biochim. Biophys. Acta 1757 (2006) 942–968.

[39] D. Bashford, M. Karplus, pK_as of ionizable groups in proteins: atomic detail from a continuum electrostatic model, Biochemistry 29 (1990) 10219–10225.

[40] D. Bashford, D.A. Case, C. Dalvit, L. Tennent, P.E. Wright, Electrostatic calculations of side-chain pK_a values in myoglobin and comparison with NMR data for histidines, Biochemistry 32 (1993) 8045–8056.

[41] G.M. Ullmann, L. Noodleman, D.A. Case, Density functional calculation of the pK_a values and redox potentials in the bovine Rieske iron–sulfur protein, J. Biol. Inorg. Chem. 7 (2002) 632–639.

[42] A.R. Klingen, G.M. Ullmann, Negatively charged residues and hydrogen bonds tune the ligand histidine pK_a values of Rieske iron–sulfur proteins, Biochemistry 43 (2004) 12383–12389.

[43] C.F. Guerra, J.G. Snijders, G. te Velde, E.J. Baerends, Towards an order-N DFT method, Theor. Chem. Acc. 99 (1998) 391–403.

[44] B. Rabenstein, G.M. Ullmann, E.-W. Knapp, Energetics of electron-transfer and protonation reactions of the quinones in the photosynthetic reaction center of Rhodopseudomonas viridis, Biochemistry 37 (1998) 2488–2495.

[45] A. Bondi, van der Waals volumes and radii, J. Phys. Chem. 68 (1964) 441–451.

[46] G.M. Ullmann, CMCT: a Monte Carlo titration program dealing with conformational variability (2005).

[47] A. Onufriev, D.A. Case, G.M. Ullmann, A novel view of pH titration in biomolecules, Biochemistry 40 (2001) 3413–3419.

[48] A.R. Klingen, E. Bombarda, G.M. Ullmann, Theoretical investigation of the behavior of titratable groups in proteins, Photochem. Photobiol. Sci. 4 (2006) 588–596.

[49] T. Ohnishi, U. Brandt, G. von Jagow, Studies on the effect of stigmatellin derivatives on cytochrome b and the Rieske iron–sulfur cluster of cytochrome c reductase from bovine heart mitochondria, Eur. J. Biochem. 176 (1988) 385–389.

[50] E. Darrouzet, M. Valkova-Valchanova, F. Daldal, The [2Fe–2S] cluster E_m as an indicator of the iron–sulfur subunit position in the ubihydroquinone oxidation site of the cytochrome bc_1 complex, J. Biol. Chem. 277 (2002) 3464–3470.

[51] A.R. Crofts, M. Guergova-Kuras, L.S. Huang, R. Kuras, Z. Zhang, E.A. Berry, Mechanism of ubiquinol oxidation by the bc_1 complex: role of the iron sulfur protein and its mobility, Biochemistry 38 (1999) 15791–15806.

[52] D. Xia, C.-A. Yu, H. Kim, J.-Z. Xia, A.M. Kachurin, L. Zhang, L. Yu, J. Deisenhofer, Crystal structure of the cytochrome bc_1 complex from bovine heart mitochondria, Science 277 (1997) 60–66.

[53] S. Iwata, J.W. Lee, K. Okada, J.K. Lee, M. Iwata, B. Rasmussen, T.A. Link, S. Ramaswamy, B.K. Jap, Complete structure of the 11-subunit bovine mitochondrial cytochrome bc_1 complex, Science 281 (1998) 64–71.

[54] X. Gao, X. Wen, C.-A. Yu, L. Esser, S. Tsao, B. Quinn, L. Zhang, L. Yu, D. Xia, The crystal structure of mitochondrial cytochrome bc_1 in complex with famoxadone: the role of aromatic–aromatic interaction in inhibition, Biochemistry 42 (2002) 11692–11702.

[55] X. Gao, X. Wen, L. Esser, B. Quinn, L. Yu, C.-A. Yu, D. Xia, Structural basis for the quinone reduction in the bc1 complex: a comparative analysis

of crystal structures of mitochondrial cytochrome bc$_1$ with bound substrate and inhibitors at the Q$_i$ site, Biochemistry 42 (2003) 9067–9080.

[56] L. Esser, B. Quinn, Y.-F. Li, M. Zhang, M. Elberry, L. Yu, C.-A. Yu, D. Xia, Crystallographic studies of quinol oxidation site inhibitors: a modified classification of inhibitors for the cytochrome *bc*$_1$ complex, J. Mol. Biol. 341 (2004) 281–302.

[57] L. Huang, D. Cobessi, E.Y. Tung, E.A. Berry, Binding of the respiratory chain inhibitor antimycin to the mitochondrial *bc*$_1$ complex: a new crystal structure reveals an altered intramolecular hydrogen-bonding pattern, J. Mol. Biol. 2005 (2005) 573–597.

[58] A. Osyczka, C.C. Moser, P.L. Dutton, Fixing the Q cycle, Trends Biochem. Sci. 30 (2005) 176–182.

[59] C. Lange, C. Hunte, Crystal structure of the yeast cytochrome *bc*$_1$ complex with its bound substrate cytochrome *c*, Proc. Natl. Acad. Sci. 99 (2002) 2800–2805.

[60] E.A. Berry, L.-S. Huang, L.K. Saechao, N.G. Pon, M. Valkova-Valchanova, F. Daldal, X-ray structure of *Rhodobacter capsulatus* cytochrome *bc*$_1$: comparison with its mitochondrial counterparts, Photosynth. Res. 81 (2004) 251–275.

[61] U. Brandt, J.G. Okun, Role of deprotonation events in ubihydro-quinone: cytochrome *c* oxidoreductase from bovine heart and yeast mitochondria, Biochemistry 36 (1997) 11234–11240.

[62] M. Brugna, S. Rodgers, A. Schricker, G. Montoya, M. Kazmeier, W. Nitschke, I. Sinning, A spectroscopic method for observing the domain movement of the Rieske iron–sulfur protein, Proc. Natl. Acad. Sci. 97 (2000) 2069–2074.